



POLITECNICO

MILANO 1863

Course of Space System Engineering and Operations

Prof. Michèle Roberta Lavagna
Academic Year 2023-2024



Project Group n. 24

Authors	Personal Code
Boccia Amelia	10996873
Cutino Sveva	11002455
D'Antonio Antonio	10992749
Harunor Tamim	10884250
Mastroleo Massimiliano	10718907
Meanti Fabio Antonio	10726189

Contents

Mission Understanding and Objectives Definition	1
1 Abstract	1
2 Mission High-Level Goals	1
3 Mission Drivers	1
4 Mission Functional Analysis	2
5 Main Phases	3
6 ConOps and Functionalities	3
7 Scientific Payload	4
7.1 Overview of the Instruments	4
7.2 Main Goals - Payload functions Correlation	6
7.3 Payload - ConOps Correlation	7
8 Mission Analysis	7
Propulsion Subsystem	8
1 Mission Trajectory Design	8
2 Reverse sizing	9
2.1 Orbit Maintenance	9
2.2 Graveyard Orbit – EOL	9
3 Propulsion System Architecture	10
3.1 Tanks	10
3.2 Valves and Plenum volume	10
3.3 Thrusters	10
3.4 Propulsion Controller Modules	11
4 Primary and Secondary Propulsion System	11
4.1 Rationale for the Adopted Design	11
5 Reverse sizing	12
5.1 Results	12
5.2 Propellant Selection	13
5.3 Tank Sizing and Positioning	13
5.4 Pressurant Selection	13
5.5 Thrusters	14
Telemetry and Telecommand Subsystem	15
1 TMTC Architecture	15
1.1 Space Segment	15
1.1.1 PLATFORM S-band TT&C (SSTL)	15
1.1.2 NAVANT	15
1.2 Ground Segment	16
1.3 Phase/ConOps and TMTC Subsystems	16
2 TMTC Reverse Sizing	17
2.1 Downlink	17
2.2 Uplink	18

2.3 Results	18
-----------------------	----

Attitude and Orbit Control Subsystem 20

1 AOCS architecture	20
1.1 Sensors	20
1.2 Actuators	20
1.3 AOCS Rationality	21
2 AOCS Sizing	22
2.1 Pointing Budgets Inputs for Each Subsystem	22
2.2 Attitude Sensors and Actuators Suite Selection According to Mode	22
2.3 Attitude Sensor Sizing According to Pointing Knowledge Needs	23
2.4 Disturbance Effects	23
2.5 Actuators Sizing	25
2.5.1 Reaction Wheels	25
2.5.2 Thrusters System	26
2.5.3 Magnetorquers	27
2.6 Mass and Power Budget	27

Thermal Control Subsystem 28

1 TCS Subsystem	28
1.1 TCS Architecture	28
1.1.1 Passive Thermal Control	28
1.1.2 Active Thermal Control	28
1.2 Thermal Environment	29
1.2.1 Thermal Flux Consideration	29
1.2.2 Considerations on GIOVE-A Thermal Environment	29
2 Sizing	30
2.1 Hot and Cold Cases Selection	30
2.2 Results	30
2.3 Adopted Control Strategy	31
2.3.1 Active Thermal Control	32
2.3.2 Passive Thermal Control	32
2.4 Mass, Power and Data Budget	33

Electric Power Subsystem 34

1 EPS Subsystem	34
1.1 EPS Design and Architecture	34
2 EPS Reverse Sizing	36
2.1 Power Budgets	36
2.2 Solar Array Sizing	37
2.2.1 Results	37
2.2.2 Positioning and Pointing	38
2.3 Battery Sizing	38
2.3.1 Results	38
2.3.2 Positioning	39
2.4 Budgets	39

Space Segment Configuration 40

1 CONF System	40
1.1 Overall Vehicle Shape and Appendages Distribution	40

1.2	Launcher Interface Location and Features	40
1.3	Vehicle Configuration in the Launcher Fairing	40
1.4	Distribution and Location of Elements	41
1.4.1	External Components	41
1.4.2	Internal Components	42
On Board Data Handling Subsystem		43
1	OBDH Subsystem	43
1.1	Architecture and Rationale	43
1.1.1	CAN Bus	43
1.1.2	OBG386	43
1.1.3	ASM	45
1.2	OBDH Reverse Sizing	45
1.2.1	OBDH Functions and Elements	45

List of Acronyms

ADC Analog to Digital Converter	GS Ground Station
AKE Absolute Knowledge Error	GSTB-V2 Galileo System Test Bed
APE Absolute Performance Error	IMU Inertial Measurement Unit
AOCS Attitude Orbit Control System	IOT In-Orbit Testing
ASM Attitude Safety Module	IOV In-Orbit Validation
BCM Battery Charge Monitor	IRES Infrared Earth Sensor
BCR Battery Charge Replacement	ITU International Telecommunication Union
BDR Battery Discharge Regulators	LEOP Launch and Early Operations
BER Bit Error Rate	LRR Laser Retroreflector
BOL Beginning Of Life	LSR Laser Ranging
BPSK Binary Phase Shifting Key	MAG Magnetic field
CAN Controlled Area Network	MEA Main Error Amplifier
CEDEX Cosmicray Energy Deposition Experiment	MEO Medium Earth Orbit
CoM Centre of Mass	MFUU Modulator, Frequency Generator and Up-converter Unit
ConOps Conceptual Operations	MLI Multi-layer Insulation
CMCU Clock Monitoring and Control Unit	MTQ Magnetorquers
CPU Central Processing Unit	NAVANT Navigation Antenna
CW Continuos Wave	NMGU Navigation Message Generation Unit
DCM Direct Cosines Matrix	NSGU Navigation Signal Generation Unit
DET Direct Energy Transfer	OBC On Board Data
DMA Direct Memory Access	OBDH On Board Data Handling
E-IOT Extended In-Orbit Testing	OCC Operation Control Centre
EDAC Error Detection aAnd Correction	OS Operation System
EIRP Effective Isotropic Radiative Power	POD Precise Orbit Determination
EOL End Of Life	PL Payload
EHS Earth Horizon Sensor	PS Propulsion Subsystem
ESA European Space Agency	QPSK Quadrature Phase Shifting Key
EPS Electric Power System	QPSK Quadrature Phase Shifting Key
FGUU Frequency Generation and Up-converter Unit	RAFS Rubidium Atomic Frequency Standard
FOV Field Of View	RAL Radio Astronomy Laboratory
GETR Galileo Experimental Test Receiver	RAM Random Access Memory
GG Gravity Gradient	RCS Reaction Control System
GIOVE Galileo In-Orbit Validation Element	RF Radio Frequency
GIOVE-A Galileo In-Orbit Validation Element-A	RO Routine Operations
GPC Giove Processing Centre	ROM Read-Only Memory
GPS Ground Position System	RTCL Resettable Timed Current Limiter
	RW Reaction Wheels

OBDH On Board Data Handling

PDM Power Distributing Module

PPT Pweak Power Tracking

PS Propulsion System

SA Solar Array

SADM Solar Array Drive Mechanism

SCOS Spacecraft Operating System

SIS Signal-In-Space

SNR Signal-to-Noise Ratio

SRP Solar Radiation Pressure

SSN Sun Sensor

SSTL Surrey Satellite Technology Ltd

TCL Timed Current Limiters

TCS Thermal Control System

TMTTC Telemetry Tracking and Command

TMU Thermal Monitoring Unit

TOT Total

TTMTC Tracking Telemetry and Telecommand System

TWTA Travelling Wave Tube Amplifier

VPN Virtual Private Network

Nomenclature

$\alpha_{coating}$	= Coating absorbivity	dpy	= Degradation over years
$\epsilon_{coating}$	= Coating emissivity	DoD	= Depth of discharge
ϵ_{Earth}	= Earth emissivity	E_m	= Specific energy
ϵ_{rad}	= Radiators emissivity	E_v	= Energy density
σ	= Boltzmann constant	\vec{F}_i	= Forces acting on the rigid body
β	= Angle between the Earth-Sun vector and orbital plane	F_e	= Solar constant
β_{critc}	= Singular configuration threshold	$F_{th_{dis}}$	= Thrusters force to counteract disturbances
μ_E	= Earth gravitational constant	$F_{th_{max}}$	= maximum thrusters force
ρ_d	= Diffusion reflection	f_{acq}	= Acquisition frequency
ρ_s	= Specular reflection	f_{typ}	= Typical frequency
θ_{rate}	= Angle rate	g_0	= Gravitational constant
θ_{slew}	= Slew angle	$h_{rw_{max}}$	= Max momentum stored by reaction wheels
η	= Line efficiency	$h_{rw_{orbit}}$	= Reaction wheels momentum in a orbit
μ	= Package efficiency	\vec{j}_B	= Residual magnetic induction
ϵ_{BOL}	= Efficiency at BOL	I	= Inertia Matrix
ρ_{Al}	= Aluminum honeycomb density	I_{max}	= S/C's maximum inertia moment
ρ_{Si}	= Silicium density	I_{sp}	= Specific impulse
θ	= Angle between array surface and Sun direction	$I_{sp_{th}}$	= Thrusters specific impulse
A_i	= Area of each surface	$I_{x,y,z}$	= Inertia moments
A_{cell}	= SA single cell area	I_D	= Inherent degradation
A_{SA}	= SA area	I_0	= Sun irradiance
$A_{SA_{real}}$	= SA real area	KIPS	= Throughput
A_{eq}	= Equivalent area of the sphere	$KIPS_{typ}$	= Typical throughput
A_{ex}	= Exposed area of equivalent sphere	L_{life}	= Lifetime degradation
A_{rad}	= Radiators area	\vec{L}	= Vector from s/c reference point to tray CoM
\vec{b}_B	= Magnetic field vector in body rf	L_{arm}	= Arm of the thrust
c	= Speed of light	M_{gas_real}	= Marginalised pressurant mass
C	= Required battery capacity	M_{prop_real}	= Marginalised propellant mass
C_A	= Battery capacity in Ah	M_{ps}	= Propulsion System mass
$C_{cell_{batt}}$	= Single battery cell capacity	M_{tank}	= tank mass
C_{string}	= Capacity of a single string	$M_{thruster}$	= Thruster mass
C_{real}	= Actual battery system capacity	m_{SA}	= SA mass
$c_{1,2,3}$	= Director cosines	m_{batt}	= Battery mass
\vec{C}	= Vector from s/c reference point to s/c CoM	MR	= Mass ratio
\vec{CoM}	= Centre of Mass position vector	$m_{prop_{des}}$	= Propellant mass for a wheel desaturation
		$m_{prop_{des}}$	= Propellant mass for station keeping
		\vec{M}	= Magnetic torque

$M_{prop_{des}}$	= Total propellant mass for desaturation	σ_{Ti}	= Titanium ultimate failure strength
$N_{batteries}$	= Number of batteries	s/c	= Spacecraft
$N_{parallel}$	= Number of SA cell in parallel	\hat{S}_B	= Sun direction in body rf
N_{real}	= Real number of SA cells	T_{tank}	= Tank temperature
N_{SA}	= Cell number for SA surface	t_{tank}	= tank thickness
N_{series}	= SA cells in series number	t_{Al}	= Aluminum thickness
$N_{series_{batt}}$	= Battery cells in series number	t_{Si}	= Silicon thickness
n_E	= Earth's rotational speed	T_{period}	= Orbit period
$n_{saturation}$	= Orbits number for desaturation	T_e	= s/c time in eclipse
n_{th}	= Number of thrusters	T_d	= s/c time in daylight
\hat{N}_{Bi}	= Surface normal vector in body rf	T_{life}	= mission duration
P_{BOL}	= SA specific power produced at BOL	T_R	= Interval in which the battery must provide power
P_d	= Power requested in daylight	$t_{des_{mag}}$	= Reaction wheels desaturation time
P_e	= Power requested in eclipse	$t_{des_{th}}$	= Desaturation time when thrusters are active
P_{EOL}	= SA specific power produced at EOL	t_{min}	= Minimum time for manoeuvre
P_{in}	= Specific SA power output	t_{slew}	= Minimum time to execute 180° slew manoeuvre
P_{SA}	= SA requested power	\vec{T}	= Rigid Body torque
P_R	= Required power for the most critical mode	T_{dis}	= Disturbances torques
P_{ps}	= Propulsion System power	$T_{des_{mag}}$	= Desired torque provided by magnetorquers
P_{tank}	= Tank pressure	$T_{mag_{max}}$	= Max torque provided by magnetorquers
$P_{thruster}$	= Thruster power	$T_{rw_{slew}}$	= Reaction wheels torque for slew manoeuvre
P_{valve}	= Valve power	$T_{th_{max}}$	= Max torque exerted by thrusters
P	= Radiation Pressure	$T_{rw_{max}}$	= Max torque exerted by reaction wheels
Q_{albedo}	= Albedo heat power	T_{SRP}	= Solar Radiation Pressure torque
$Q_{emitted}$	= Heat emitted by the Earth	T_{GG}	= Gravity Gradient torque
Q_{IR}	= Earth's infrared heat power	T_{MAG}	= Magnetic Field Torque
$Q_{heaters}$	= Heaters heat power	T_{TOT}	= Total Torque
Q_{Sun}	= Sun heat power	T_{DS}	= Deep space temperature
Q_{int}^{hot}	= Internal heat power worst hot case	T_{Earth}	= Earth temperature
Q_{int}^{cold}	= Internal heat power worst cold case	T_{Max}	= Maximum temperature
$Q_{s/c}^{hot}$	= Spacecraft heat power worst hot case	T_{Min}	= Minimum temperature
$Q_{s/c}^{cold}$	= Spacecraft heat power worst cold case	T_{sc}^{cold}	= Temperature in the worst cold case
\vec{r}_i	= Distance between pressure centres and CoM	T_{sc}^{hot}	= Temperature in the worst hot case
R	= Satellite-Earth centre distance	r_{tank}	= tank radius
$R_{specific}$	= Specific gas constant	$V_{gas,i}$	= pressurant initial volume in the tank
ρ_{prop}	= propellant density	V_{prop_real}	= Marginalised propellant volume
ρ_{Ti}	= Titanium density	V_{tank_real}	= Marginalised tank volume

V_{batt} = Battery volume

$V_{real_{batt}}$ = Real battery voltage

$V_{cell_{SA}}$ = Solar Array single cell voltage

$V_{cell_{batt}}$ = Battery single cell voltage

V_{syst} = System voltage

$V_{syst_{batt}}$ = System voltage for battery

X_d = Line efficiency in daylight

X_e = Line efficiency in eclipse

List of Figures

1	<i>Figure 1</i> : Function Tree	2
2	<i>Figure 2</i> : ConOps	3
3	<i>Figure 3</i> : Payload location in the spacecraft	5
4	<i>Figure 4</i> : ΔV bar-diagram	8
5	<i>Figure 5</i> : Propulsion system schematic ^[17]	10
6	<i>Figure 6</i> : The variants of SSTLs low cost resistojet ^[20]	14
7	<i>Figure 7</i> : ΔV bar-diagram	14
8	<i>Figure 8</i> : TMTC Architecture ^[21]	15
9	<i>Figure 9</i> : Ground Segment Architecture	16
10	<i>Figure 10</i> : S-patch antenna ^[21]	19
11	<i>Figure 11</i> : TMTC architecture ^[26]	19
12	<i>Figure 12</i> : Nominal Pointing Scheme ^[36]	21
13	<i>Figure 13</i> : CoM location ^[40]	23
15	<i>Figure 14</i> : Orbiting spacecraft heating simplified overview ^[43]	28
16	<i>Figure 15</i> : GIOVE-A Resistojet with thermocouples ^[59]	33
17	<i>Figure 16</i> : Giove-A EPS block diagram ^[7]	34
18	<i>Figure 17</i> : BCR Operation and Battery Charging Sequence ^[66]	35
19	<i>Figure 18</i> : GIOVE-A solar array ^[67]	37
20	<i>Figure 19</i> : PDM and MEA ^[76]	39
21	<i>Figure 20</i> : General Giove-A configuration	40
22	<i>Figure 21</i> : Giove-A "unpacked" configuration	40
23	<i>Figure 22</i> : GIOVE-A "packed" configuration and connection with Soyuz/Fregat launcher upper stage	40
24	<i>Figure 23</i> : External Elements Giove-A	41
25	<i>Figure 24</i> : Internal Elements Giove-A	42
26	<i>Figure 25</i> : Overall Giove-A CAN bus connections	43
27	<i>Figure 26</i> : Giove-A actual OBC386 ^[83]	44
28	<i>Figure 27</i> : GIOVE-A OBC386 schematics ^[87]	44

List of Tables

1	<i>Table 1</i> : Links between phases, ConOps and functionalities	4
2	<i>Table 2</i> : Link between mission goal and payload	6
3	<i>Table 3</i> : Links between Phases/ConOps and Payload	7
4	<i>Table 4</i> : Orbit characterization	7
5	<i>Table 5</i> : Description of the perturbation ^{[13][14]}	8
6	<i>Table 6</i> : Preliminary values of ΔV	10
7	<i>Table 7</i> : Typical SSTL propulsion solutions ^[17]	12
8	<i>Table 8</i> : Performance and Tank Parameters	12
9	<i>Table 9</i> : Results	12
10	<i>Table 10</i> : Phase/ConOps and TMTC subsystems ^{[25][26]}	17
11	<i>Table 11</i> : Downlink input data	17
12	<i>Table 12</i> : Uplink input data	18
13	<i>Table 13</i> : Downlink results	18
14	<i>Table 14</i> : Uplink results	18
15	<i>Table 15</i> : Detailed specifications of sensors ^{[29][30][31]}	20
16	<i>Table 16</i> : Attitude control delta V Requirements ^[35]	20
17	<i>Table 17</i> : Specifications of the actuators ^{[32][33][34]}	21
18	<i>Table 18</i> : Input Pointing Budget ^{[37][36]}	22
19	<i>Table 19</i> : Maximum values of the torques	24
20	<i>Table 20</i> : Sizing input data and numerical results	25
21	<i>Table 21</i> : AOCS Mass and Power Budget	27
22	<i>Table 22</i> : Internal power generated [W]	30
23	<i>Table 23</i> : Sizing numerical results	30
24	<i>Table 24</i> : Real temperature ranges of GIOVE-A components	32
25	<i>Table 25</i> : Mass and Power budgets	33
26	<i>Table 26</i> : Expected and measured current values ^[66]	34
27	<i>Table 27</i> : Power budget per phase per mode	36
28	<i>Table 28</i> : SA sizing input data and results	37
29	<i>Table 29</i> : EPS mass budget ^{[76][77][42]}	39
30	<i>Table 30</i> : EPS power budget ^{[67][42]}	39
31	<i>Table 31</i> : PS volume budget ^[76]	39
32	<i>Table 32</i> : OBDH functions and elements	45
33	<i>Table 33</i> : OBDH sizing results per mode	46

MISSION UNDERSTANDING AND OBJECTIVES DEFINITION

1 Abstract

GIOVE-A is one of the two satellites developed by Surrey Satellite Technology Ltd for ESA's GIOVE program. This mission was planned to last from 2005 to 2008 but it was extended until 2012. GIOVE-A was officially decommissioned in 2021.

Galileo is a fully autonomous and interoperable worldwide satellite navigation system, broadcasting global navigation signals for high-performance services. As the first step in validating the Galileo system, GIOVE-A, alongside GIOVE-B satellite, played a key role in testing the functionality and interoperability of in-orbit technologies for the Galileo navigation system. Our study aims to conduct a reverse engineering analysis of the GIOVE-A mission, focusing on the sizing and performance of its subsystems, to gain insights into achieving mission objectives and enhancing future space missions^{[1][2]}.

2 Mission High-Level Goals

GIOVE-A is Europe's first navigation satellite and the first MEO orbiter for the continent. As a crucial component of the Galileo programme, it leads the way for the next generation of navigation technology. The mission aims to achieve the following goals^{[3][4]}:

- **Securing the frequency filings with ITU**

The main objective of the GIOVE-A mission is to secure the frequencies bands allocated by ITU for the Galileo programme within the assigned timeframe in order to fulfil the time requirement imposed by the ITU.

- **Enable SIS experimentation for the Galileo Navigation System**

GIOVE-A is the pathfinder platform for the IOV phase, essential for the advancement of the Galileo programme. The satellite aims to validate the Galileo signals in space, ensuring their performance, reliability, accuracy and compatibility with existing GPS and future Galileo satellites.

- **Testing of key technologies for future navigation missions**

Additionally, GIOVE-A enables in-space testing for cutting-edge technologies, notably the rubidium atomic clocks and the Galileo navigation signal generators, both of which had never flown in space before this mission.

- **Characterise MEO environment**

Another objective of the GIOVE-A mission is the complete characterisation of the radiation environment of the orbital region designated for the future orbits of the Galileo constellation satellites.

- **Test the receivers on the ground**

Concerning the ground segment, the main objective of the mission is to ensure the functionality and performance of the Galileo signals receivers on ground.

3 Mission Drivers

The critical factors and constraints which drive the design philosophy and significantly influence the technical design, planning, and execution of the GIOVE-A mission are^[5]:

- **Securing the frequency filings for Galileo program within the allocated timeframe**

The ITU assigns specific frequency bands to users who apply for them with the requirement of securing them within a 7 years timeframe. During the development of the Galileo program, it was vital to launch a pilot satellite (GIOVE-A) rapidly in order to secure the Galileo frequency filings and subsequently validate the Galileo signal transmission technology in a relevant environment (space).

- **Surviving and operating in the MEO environment for at least 2 years**

MEO region includes two zones rich of energetic charged particles above the equator known as the Van Allen radiation belts. These belts pose a serious threat to the on-board electronic systems due to the high energy radiation exposure. In order to carry out GIOVE-A's validation mission it is crucial that the spacecraft is able to survive and operate in this harsh environment for the entire duration of the planned mission (2 years).

4 Mission Functional Analysis

The following figure shows the GIOVE-A mission functional analysis^[6].

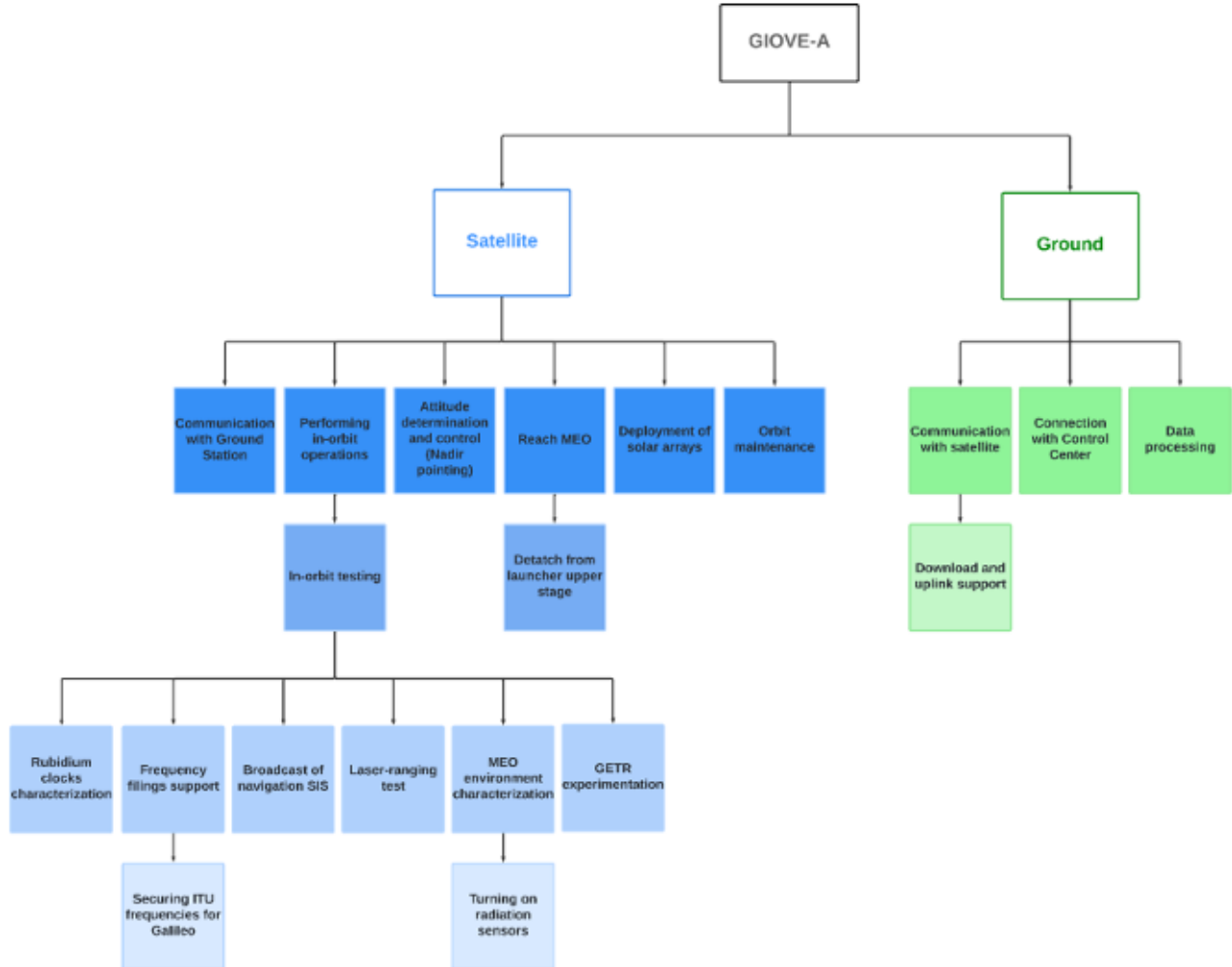


Figure 1 : Function Tree

5 Main Phases

The GIOVE-A mission is divided into five main phases: LEOP, IOT, E-IOT, Routine Ops and EOL^[7].

- **LEOP:** This phase comprehend the Launch and early operations needed to start the mission. The launch occurred on December 28, 2005, at 5:19 UT, from the Baikonur Cosmodrome utilising a Soyuz Fregat launcher. The initial contact with the Ground Station enabled preliminary checkouts and initiated the nominal operations.
- **IOT:** The second phase consists in performing the in-orbit testing, necessary to assess the GIOVE A goals. After the first signal, all Galileo signals were exercised securing Europe's frequency filing allocation for Galileo assigned by the ITU, which was informed, through the IOT review, on March 8, 2006, that all frequencies of Galileo had been put in use.
- **E-IOT:** The third phase is an extension of the previous one, in which several activities were carried out, such as:
 - The first clock characterisation campaign, whose measurements showed that the rubidium clocks were operating as expected.
 - The satellite laser-ranging campaign, whose data were used for Precise Orbit Determination (POD) analysis (from 22 May, 2006 until 24 July, 2006).
 - The GETR experimentation, which demonstrated the interoperability between Galileo and GPS (from May 2006 until June 2006).
- **Routine Ops:** After July 24, 2006 GIOVE-A entered a routine operation phase during which GIOVE-A continued to carry out its main tasks (MEO and rubidium clocks characterisation, Galileo-like signal transmission).
- **EOL:** GIOVE-A mission was planned to operate for 27 months after which the satellite would have been positioned on a graveyard orbit for its disposal at 23'300 km of altitude. However, because of its great success and the good state of its systems, the mission was extended multiple times for a total duration of 78 months. In June 2012, ESA formally ended the mission and SSTL took over operations, until GIOVE-A was officially decommissioned on November 24, 2021 due to the obsolescence of the on-board computer.

6 ConOps and Functionalities

The following figure shows the ConOps timeline^[7].

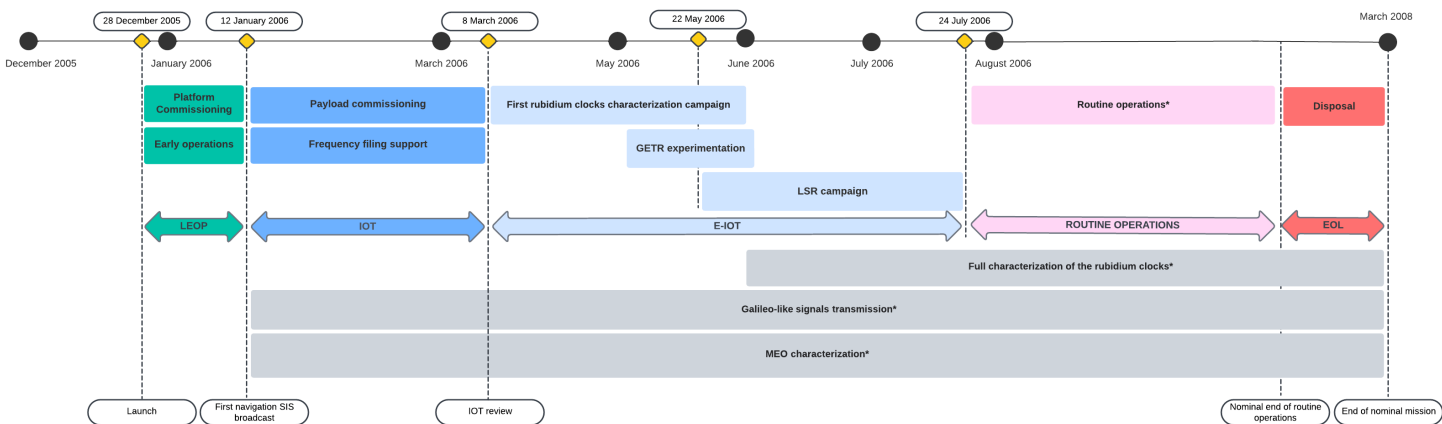


Figure 2 : ConOps

Furthermore, *Table 1*, presents the link between phases, ConOps and functionalities^{[8][9]}.

Phase	ConOps	Functionalities
LEOP	<ul style="list-style-type: none"> • Launch • Early Operations • Platform Commissioning 	<ul style="list-style-type: none"> • Detachment from upper stage; reaching MEO • Deployment of solar arrays; attitude determination and control; activation of radiation monitoring sensors (Merlin and CEDEX) • Establishing contact with Ground Station
IOT	<ul style="list-style-type: none"> • Payload Commissioning • Frequency filing support • IOT Review 	<ul style="list-style-type: none"> • Communication with Ground Station • Broadcasting of navigation SIS • Securing ITU frequencies for Galileo
E-IOT	<ul style="list-style-type: none"> • Rubidium clock characterisation campaign • GETR experimentation • LSR campaign 	<ul style="list-style-type: none"> • In-orbit testing • Data processing
Routine Operations	<ul style="list-style-type: none"> • Galileo-like signals transmission • MEO characterisation • Full characterisation of the rubidium clocks 	<ul style="list-style-type: none"> • Broadcasting of navigation SIS • Utilisation of radiation sensors (Merlin and CEDEX) • In-orbit testing
EOL	<ul style="list-style-type: none"> • Disposal 	<ul style="list-style-type: none"> • Orbit change; de-activation

Table 1 : Links between phases, ConOps and functionalities

7 Scientific Payload

7.1 Overview of the Instruments

The scientific payload on GIOVE-A consists of three main areas of focus: navigation, radiation monitoring, and experimental. This is to facilitate the overall objectives of the mission.^{[10][11]}

NAVANT (Navigation Antenna)

It is a phased array of individual L-band elements, also called isoflux. They illuminate the whole world below. It consists of 36 self-diplexed and stacked patch radiators fed by two independent Beamforming Networks which operate at low and high frequency band. It generates an isoflux pattern to equalize the power level it receives on ground, and a broadband frequency response required by the Galileo mission with optimum performance.

NSGU (Navigation Signal Generation Unit)

To execute the function of generating two representative Galileo signals, NSGU has two units with a mass of < 1.4 kg, and a power consumption of < 20 W. It, thus, receives the navigation message information, generates navigation message while modulating a set of pseudo random noise codes and, finally, mixes different signal components for base-band or IF interface with the up-conversion unit.

FGUU (Frequency Generation and Up-converter Unit)

The mission has two FGUU devices on board to generate a simple Galileo signal and a more representative one. FGUU mainly receives signals from NSGU, generates LO signals for translating frequency, conditions, then, filters signals to meet system requirements, and generates NSGU reference clock signal.

RAFS (Rubidium Atomic Frequency Standard)

There are two clocks on board GIOVE-A, and they are in redundant configuration to account for failure and increase reliability. The clocking system installed is RAFS. A RAFS unit weighs 3.3 kg.

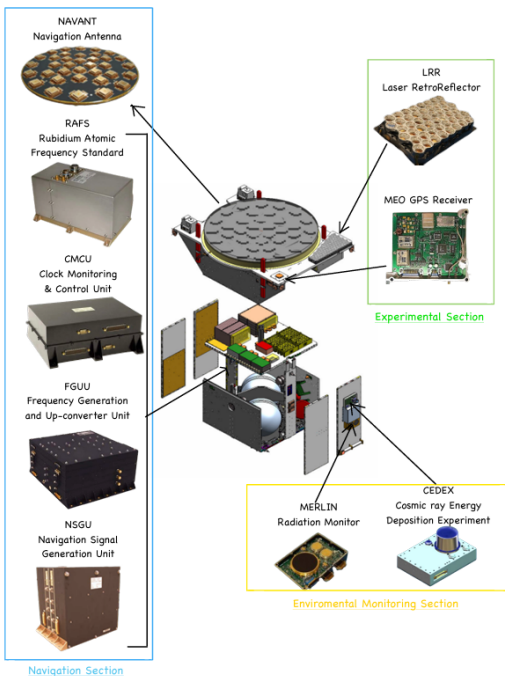


Figure 3 : Payload location in the spacecraft

a mass of 1.7 kg and a power of 2.5 W. The dimensions are crucial for its ideal placement on the spacecraft. This instrument measures the internal charging currents to get the ambient energetic electronic fluxes, energetic proton fluxes, cosmic ray ion linear energy transfer spectra, and total ionizing dose rates in silicon. This leads to properly gauge the radiation hazards in MEO. It has a mass of 1.7 kg, a power consumption of < 2.5 W and a 24-hour storage at standard sampling rate. Because of its direct interaction with the MEO orbit environment, it has an additional mass for boxed radiation shielding. Total dose is measured in krad (SiO₂) at two shielding depths. Merlin has two particle telescopes: one for measuring heavy ion LET (linear energy transfer), and the other for proton counting.

CEDEX (Cosmic ray Energy Deposition Experiment)

The objective of this instrument is to monitor high-energy (40 - 50 MeV) proton fluxes. It also utilizes the observed particle LET (Linear Energy Transfer) spectrum to characterize the MEO orbital radiation environment. The dose rate-induced photocurrents are monitored by PIN diodes at 4 different shielding depths which enables characterization of the dose-depth curve. It has a mass of 2.05 kg and a power consumption of 4.2 W at 38 V.

LRR (Laser Retroreflector)

This instrument is an integrated array of 76 coated corner cube reflectors. They are placed on the nadir side of the spacecraft. The goal is to find the laser ranging for precise orbit determination analysis. The precision of the measurement is instantaneous and millimeter level – which leads to a more accurate clock characterization.

MEO GPS Receiver

This instrument is installed to experiment with autonomous localization in the MEO. The GPS measurements get recorded and downloaded to a ground station for post processed orbit recovery. For operating in MEO orbits, it's standard that the receiver has a medium gain patch antenna, OCXO (Oven Controlled Crystal Oscillator), radiation mitigation and FARM (Ferro-electric Random Access Memory). For GIOVE-A the receiver contains similar features where it has a larger patch antenna installed with a parasitic element. It has to track the signals from the GPS satellites positioned on the far side of the Earth – weaker signal reception. The small physical size of the receiver allows for overall shielding without any undesired mass increase.

CMCU (Clock Monitoring and Control Unit)

This unit generates the standard reference frequency at 10.23 MHz (Master Clock). The time-keeping system is made of RAFS clocks, and this unit provides the master clock. It carries out a phase comparison system in order to control the RAFS clocks. Additionally, it interfaces with the onboard data handling system.

NMGU (Navigation Message Generation Unit)

This unit is responsible for generating signature Galileo radio frequencies in two non-identical navigation frequency bands, namely: upper and lower band, center frequencies at 1575 MHz and at 1191 MHz.

MFUU (Modulator, Frequency Generator and Upconverter Unit)

There are two units of MFUU in this mission where their function is to amplify the output radio frequency carriers of the RNSS signals. The signals from the upper bands are E2, L1, and E1, lower band E5a/b and E6.

Merlin

This is essentially a compact space weather monitor with a mass of 1.7 kg and a power of 2.5 W. The dimensions are crucial for its ideal placement on the spacecraft. This instrument measures the internal charging currents to get the ambient energetic electronic fluxes, energetic proton fluxes, cosmic ray ion linear energy transfer spectra, and total ionizing dose rates in silicon. This leads to properly gauge the radiation hazards in MEO. It has a mass of 1.7 kg, a power consumption of < 2.5 W and a 24-hour storage at standard sampling rate. Because of its direct interaction with the MEO orbit environment, it has an additional mass for boxed radiation shielding. Total dose is measured in krad (SiO₂) at two shielding depths. Merlin has two particle telescopes: one for measuring heavy ion LET (linear energy transfer), and the other for proton counting.

CEDEX (Cosmic ray Energy Deposition Experiment)

The objective of this instrument is to monitor high-energy (40 - 50 MeV) proton fluxes. It also utilizes the observed particle LET (Linear Energy Transfer) spectrum to characterize the MEO orbital radiation environment. The dose rate-induced photocurrents are monitored by PIN diodes at 4 different shielding depths which enables characterization of the dose-depth curve. It has a mass of 2.05 kg and a power consumption of 4.2 W at 38 V.

LRR (Laser Retroreflector)

This instrument is an integrated array of 76 coated corner cube reflectors. They are placed on the nadir side of the spacecraft. The goal is to find the laser ranging for precise orbit determination analysis. The precision of the measurement is instantaneous and millimeter level – which leads to a more accurate clock characterization.

MEO GPS Receiver

This instrument is installed to experiment with autonomous localization in the MEO. The GPS measurements get recorded and downloaded to a ground station for post processed orbit recovery. For operating in MEO orbits, it's standard that the receiver has a medium gain patch antenna, OCXO (Oven Controlled Crystal Oscillator), radiation mitigation and FARM (Ferro-electric Random Access Memory). For GIOVE-A the receiver contains similar features where it has a larger patch antenna installed with a parasitic element. It has to track the signals from the GPS satellites positioned on the far side of the Earth – weaker signal reception. The small physical size of the receiver allows for overall shielding without any undesired mass increase.

7.2 Main Goals - Payload functions Correlation

The intent of this paragraph is to correlate the aims of the mission discussed in Section 2 with the related payloads that favor the achievement of these objectives^[7].

Science Objectives	Measurements Objectives
Securing the frequency filings with ITU and enable SIS experimentation for the Galileo Navigation System	The commissioning of the navigation payload started with a full checkout of the low-power equipment and then with the high-power equipment. GIOVE-A transmits its first SIS navigation message using the navigation unit composed of NAVANT, NSGU, FGUU, MNGU and MFUU. In the weeks following the initial signal, all the Galileo signals were exercised - thereby securing Europe's frequency allocation filing for Galileo
Testing of key technologies for future navigation missions	<p>The technologies that have been successfully tested on board this satellite during its mission are:</p> <ul style="list-style-type: none"> • laser-ranging test: LRR, RAFS, CMCU; • radiation monitoring: Merlin, CEDEX; • clock characterization campaign: RAFS, CMCU; • monitoring of rubidium clocks: RAFS; • testing GPS receivers in missions above 20000km altitude: MEO GPS receivers
Characterize MEO environment	Using Merlin and CEDEX, it was possible for the satellite to collect data for more than ten years on the environment in MEO, showing some interesting features such as the "electron desert" and providing information that have brought at a new model of the outer Van Allen belt electron fluxes, used to improve future satellite designs
Test the receivers on the ground	Once acquired all the data concerning the various missions and the various objectives of the satellite in orbit, they are sent to the various ground stations that will provide the download and processing. The tools from which they will receive information are the MEO GPS receivers, Merlin and CEDEX for the study of the environment in MEO and the navigation unit for the tests concerning the precise identification of an object in space within a certain tolerance

Table 2 : Link between mission goal and payload

7.3 Payload - ConOps Correlation

The final orbit was reached 222 minutes after lift-off. The first ground-space contact was established after two minutes and then the solar array deployment was initiated and completed within two hours. In the following table P/Ls and Phase/ConOps correlation is reported^[12].

Science Objectives	Measurements Objectives
LEOP	<ul style="list-style-type: none"> Navigation instrument commissioning: complete check-out of low-power and then of high-power equipment; First navigation SIS (Signal-In-Space); Merlin and CEDEX powered; they started working the very next day after lift-off.
IOT	<ul style="list-style-type: none"> Payload Commissioning; Navigation Payload secured ITU frequency.
E-IOT	<ul style="list-style-type: none"> Laser-ranging test successful provided results well within expectation; Testing of GPS receiver. It worked just for 90 minutes due to the incompatibility with the main transmitted payload; Data of environmental payload have been analysed granting their good quality; First clock characterization campaign showed that RAFS are operating as expected.
Routine Operations	<ul style="list-style-type: none"> Environmental and Navigation payload kept operating; Transmission of first navigation signal, containing information about GIOVE-A position: before this achievement the satellite had only broadcasted the data to measure the receiver-satellite distance.

Table 3 : Links between Phases/ConOps and Payload

8 Mission Analysis

The orbit selection answers to the goals, already discussed in Section 2.

Altitude	Inclination	Period	Orbit Geometry
23258 km	56°	14 h 22 min	Near-circular

Table 4 : Orbit characterization

The chosen altitude let correctly characterize the MEO environment. In addition, the choice of a near-circular orbit with an inclination of 56° guarantees total coverage during the whole mission, to avoid losses in telecommunication.

PROPELLION SUBSYSTEM

1 Mission Trajectory Design

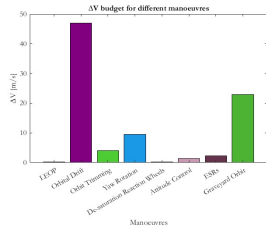


Figure 4 : ΔV bar-diagram

The design of the mission trajectory is a crucial phase in which the various part of the mission are analysed and optimized in order to achieve the set objectives with the necessary efficiency and precision.

During the space mission, Giove-A faces several key phases, each with specific ΔV requirements to meet orbital positioning, orbit change, trajectory correction, or other critical operations. These phases include the orbital transfer manoeuvre, operational orbit entry, any orbital corrections during operational life, and finally the decommissioning or deorbiting phase^[7].

Phase	ΔV [m/s]	Description of the Perturbation
LEOP	0.21	The satellite must be stabilized and correctly oriented to counteract the instabilities due to the accelerations of the launch itself, the acquisition and the solar control, the calibration of the sensors and the thermal control.
Orbital Drift	47	This manoeuvre allows the satellite to vary its relative position with respect to Giove-B in a time-controlled manner. Its purposes are: orbital alignment, orbital retention, orbital resettlement and orbital correction.
Orbit Maintenance	4	This budget refers to the orbital trimming (600m accuracy): series of orbital manoeuvre performed to adjust the orbit, compensating the perturbations and deviations of the satellite to obtain a desired orbital position and optimize its performance.
	9.54	Budget requested for parasitic torque corrections through Yaw rotations: attitude control practice helping to maintain the stability of the attitude and efficiency of space operations.
	0.20	Budget requested for de-saturation of reaction wheels: refers to a procedure used to correct or compensate the excess angular velocity accumulated in the reaction wheels of a satellite, ensuring that it is able to respond promptly and accurately to control commands during its space mission.
	1.44	Budget requested for Attitude Control through thruster: technique that uses the engines for generating a controlled thrust that allows you to change the orientation and attitude of the vehicle. The attitude control manoeuvre carried out concern stabilization, change and orientation and finally orbital corrections.
	2.22	10 ESRs : Expendable Secondary Wheels, these are secondary reaction wheels used in satellites for attitude and orientation control used to make adjustments in the orientation.
EOL	23	Budget requested to re-position the satellite in a graveyard orbit that is usually at a greater distance than the initial orbit, with orbital parameters that minimize interactions with other space objects to reduce the risk of accidental collision with other operational satellites or space debris.

Table 5 : Description of the perturbation^{[13][14]}

2 Reverse sizing

The total ΔV for complete orbit maintenance during the Giove-A mission is 87.61 m/s and it refers to a nominal mass of 600 kg. Before the actual launch of the satellite a cost forecasting process was drawn up finding a minimum ΔV budget of 93.5 m/s. The team aims to reverse engineer the ΔV budget for the orbit maintenance and EOL phases of the mission so as to demonstrate and justify its values c.

2.1 Orbit Maintenance

Since the whole mission regards the MEO orbit validation a crucial aspect of the design is to ensure the station keeping of the satellite. This is achieved through a meticulous analysis of the expected environment, focusing on the intensity of the disturbances and how they affect the satellite behaviour.

Through the ephemerides we get the position in space, with respect to the Sun, of GIOVE-A and Earth during the mission, right after the arrival in the target orbit; then we study their relative positions, especially looking for possible eclipse moments, in which the solar radiation pressure will not directly affect the satellite. Now we define the acceleration that will make it shifts from its trajectory^[15].

Hypothesis for the computation:

- Perturbations which are less relevant at our altitude, like atmospheric drag, have been neglected;
- Optical properties assumed are those of silicon solar panels;
- Solar radiation pressure is constant;
- 1 AU as the average Sun-Earth distance.

For what concern with the time window we considered the whole mission period, avoiding:

- Time requested to achieve the target orbit: 222 minutes;
- Manoeuvre time for orbital drift: one month.

Once we have everything to compute the acceleration due to Sun presence, we integrate its values at multiple instances of the trajectory, to get the ΔV that we need to compensate for orbit maintenance.

All the calculations have been carried out using MATLAB coding environment.

Finally, we found an hypothetical value of $\Delta V_{tot} = 6.5563 \text{ m/s}$, about $\Delta V = 0.0023 \text{ m/s}$ for each orbit.

Considering ESA standard for the accuracy of the ΔV parameter, a margin of 10 % is added to the previous results because we have adopted an analytical approach, having so:

$$\Delta V_{tot} = \Delta V + 10\% \Delta V = 7.2119 \text{ m/s.}$$

It is close enough to the real value of $\Delta V = 4 \text{ m/s}$ as seen in Table 1 above: the slight difference can be imputed to the hypothesis on the optical properties, the constant solar radiation pressure, and the neglected disturbances, that could attenuate or empathize the total effect of perturbations^[16].

2.2 Graveyard Orbit – EOL

After the completion of the 27-month nominal mission in MEO orbit and so after the decommissioning, the GIOVE-A satellite performs a manoeuvre that will lead it to position itself in an orbit that has got a higher altitude called 'graveyard'. This orbit, located about 100km above the previous orbit in MEO, is safer from the point of view of collisions with other active satellites in their operating orbits or space debris and is a fundamental part of the practices of responsible space management. In this case the graveyard orbit is used when the change in velocity required to perform a de-orbit manoeuvre is too large.

For reaching that altitude of 23222 km, the satellite must perform an orbital transfer manoeuvre. To calculate the ΔV budget, it is necessary to make assumptions in order to simplify the calculations:

- Initial and final orbits are considered circular and coplanar, without taking into account the probable difference in inclination between the two;
- Hohmann-type transfer: perform a double pulse manoeuvre.

The result obtained represents the preliminary value of ΔV required for this transfer:

$$\Delta V = (\Delta V_{1_{transferorbit}} - V_{1_{MEOorbit}}) + (\Delta V_{2_{Graveyardorbit}} - V_{2_{transferorbit}}) = 6.185 \text{ m/s}$$

Although our result is derived from an analytical calculation without stochastic components, the use of different assumptions to adopt the method of calculation described requires the application of a margin equal to 100% of the result, as suggested by ESA standards.

	Eccentricity [-]	Semi-major axis [km]	V_1 [m/s]	V_2 [m/s]
MEO orbit	0	23258 + 6371	3670.0	3670.0
Transfer orbit	0	23300 + 6371	3673.1	3660.7
Graveyard orbit	7.0826e-04	23279 + 6371	3663.8	3663.8

Table 6 : Preliminary values of ΔV

$$\Delta V = \Delta V + 100\% * \Delta V = 12.37 \text{ m/s}$$

This result is different from that verified through experimental data of 23m/s. The reasons for this discrepancy may be related to the assumptions made for the calculation of the orbital transfer through the transfer to Hohmann and for the fact that part of the ΔV budget is used to maintain the orbit of graveyard.

3 Propulsion System Architecture

GIOVE-A satellite is equipped with a liquid butane propulsion system which has been developed thanks to the heritage of several SSTL missions. The study of the propulsion subsystem aims to analyse and highlight its characteristics and reasoning of the rationale behind the design decisions that were made^[17].

3.1 Tanks

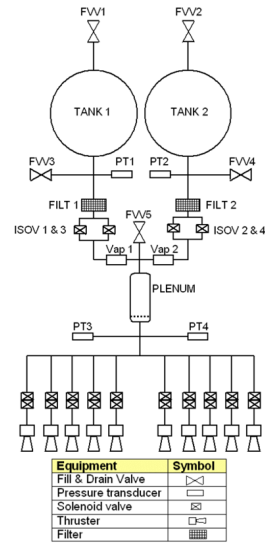
The propulsion system is equipped with two spherical tanks containing 25 kg of liquid butane each. The butane is kept under nominal storage conditions with a maximum pressure of 4 bar equivalent to its own vapour pressure, at a temperature of 40°C. This eliminates the necessity for complex pressurisation mechanisms which would increase the system's mass and cost. Solenoid valves are used to isolate the tanks, preventing unwanted propellant transfer between them. Additionally, pressure transducers are placed next to each tank to enable constant pressure monitoring within them.

3.2 Valves and Plenum volume

The propellant is fed from each tank through a filter, parallel solenoid isolation valves (to give fail closed redundancy), a vaporiser and a plenum volume. The tank isolation valves also act as pressure regulation valves and are controlled using the feedback from the pressure transducers connected to the plenum chamber. The system is designed to prevent liquid phase propellant being fed into the thrusters since this would compromise the propulsion system performance. Therefore, the propellant vapour pressure in the plenum and lines must be controlled to keep it lower than the butane condensation pressure. The vaporiser is used to vaporise any liquid phase propellant exiting the regulation solenoid valve going into the plenum chamber. In the control loop, two pressure limits are established. If the plenum pressure drops below the lower boundary, the tank isolation valve opens, allowing the propellant to flow and pressurize the plenum. Once the upper boundary is reached, the tank isolation valve shuts. As the thrusters consume the propellant, the plenum pressure decreases until it hits the lower limit again. At this point, the microcontroller instructs the tank isolation valve to open, initiating the re-pressure process once more. The pressure boundaries for Giove-A are typically set between 0.9 and 1.1 bar, but these can be adjusted by the spacecraft operator via telecommand^[18].

3.3 Thrusters

The spacecraft is equipped with ten T-15 thrusters designed by SSTL, all linked to a singular pipe run through dual seat valves. These valves are thermally isolated from the heater chamber assembly, also known as the resistojet, which is mounted on the spacecraft's external surface. The pipework is fitted with pressure transducers and temperature sensors, along with a test port for ground testing operations^{[19][20]}.

Figure 5 : Propulsion system schematic^[17]

3.4 Propulsion Controller Modules

The propulsion system is managed by two Propulsion Controller Electronics modules. Each of these controllers is responsible for operating half of the propulsion system, which includes five thruster valves and heaters, as well as two tank isolation valves. In case of failure of one of the propulsion controller modules, the other one is capable of supplying five thrusters from either of the propellant tanks, ensuring the mission's completion. If Propulsion controller 1 is being used it will use the output of the line transducer PT3 to operate either isolation valve 1 to draw from tank 1, or isolation valve 2 to draw from tank 2.

4 Primary and Secondary Propulsion System

The ΔV requirements for the GIOVE-A mission have been previously addressed in Section 1. Given its planetary nature, the relatively low ΔV values derived from the MA were expected.

Primary Propulsion Solution

In the specific case of GIOVE-A satellite, no proper primary propulsion system is installed on board, as the mission does not require significant manoeuvres. To achieve the nominal orbit, the third stage of the Soyuz-FREGAT launcher is utilised, effectively serving the function of the primary propulsion system.

Secondary Propulsion Solution

The on-board propulsion unit consists of a liquid butane system with resistojet thrusters. This type of propulsion system provides low ΔV suited for fine attitude control (Nadir pointing), orbit maintenance, small orbital changes. Therefore, the on-board propulsion unit can be classified as a secondary propulsion system.

4.1 Rationale for the Adopted Design

The primary requirements of the GIOVE-A propulsion system are the following:

- Ensure operational longevity of at least 27 months in the MEO environment
- Low cost and minimization of the project schedule
- Granting personnel safety by mitigating risks and providing high reliability

The satellite employs a liquid butane propulsion system, chosen for its reliability and suitability for the satellite's mission to MEO. An initial trade-off was performed, examining both conventional propulsive options and those belonging to the SSTL's heritage. The assumptions made for the initial design are:

spacecraft launch mass: 400 kg	minimum ΔV required: 93.5 m/s
propellant tank volume: 120 litres	propellant mass: not critical, volume limited

These are based on SSTL's GEMINI (GEostationary MINIsatellite) programme's platforms. Moreover, the tanks used were derived from a hydrazine tank on Exosat, from PSI (Pressure Systems, Inc.) by removing the elastomeric diaphragm.

The rationale behind the choice of using well established technologies is closely linked to one of the drivers of the GIOVE-A mission, which is to minimise the mission schedule in order to claim the Galileo frequencies on time. Moreover, the satellite featured a modular design with separate propulsion, avionics, and payload bays, which facilitated ease of assembly, integration, and testing. This modular approach also allowed for a level of redundancy and reliability that was necessary for the satellite's long-term mission.

The main element that influenced the whole propulsion system design is the choice of the propellant. From the computations based on the previously mentioned initial assumptions, the system required a performance level somewhere between conventional cold gas nitrogen and hydrazine systems.

High-pressure nitrogen with high power resistojet thrusters could nearly meet the specific impulse requirement, however the absence of an appropriate tank design, which would be extremely heavy if it existed, ruled out this option. On the other hand, hydrazine could easily meet the ΔV requirements with tanks at $\frac{1}{4}$ capacity (22.5kg), based on the GEMINI platform, but it had significant costs and SSTL lacked the necessary infrastructures to deal with it.

Therefore, to meet the requirements, there was the need to use liquified gases with resistojet heaters. The

typical SSTL propulsion solutions were:

Propellant	ΔV [m/s]	Comments
Ammonia	147.7	Toxicity issues, high cost, compatibility issues
Propane	99.8	Flammability issues
Butane	117.7	Flammability issues
Carbon Dioxide	112.3	High pressure (50 Bar at 20°C), hence the need of new qualified tank
Nitrous Oxide	109.3	High pressure (52 bar at 20°C), hence the need of new tank

Table 7 : Typical SSTL propulsion solutions^[17]

All the proposed solutions satisfy the ΔV requirements within the fixed volume constraint. Upon reviewing the characteristics of each propellant as presented in Table 2, it becomes evident that the optimal solution for the GIOVE-A mission is the implementation of a liquid butane propulsion system. This choice offers a significant reduction in both cost and risk compared to hydrazine, aligning well with the propulsion system's requirements. Liquid butane has a storage density of $0.53\text{g}/\text{cm}^3$ and a theoretical specific impulse of 70 seconds. This results in a density Isp (impulse per unit volume of propellant) of 362 Ns per litre, significantly higher than nitrogen's 165 Ns per litre. Consequently, butane can be stored in a considerably smaller volume compared to nitrogen. Furthermore, butane's low storage pressure is another advantage: at 20°C, its vapour pressure is 2.1 bar absolute. This low pressure offers two key benefits:

- Traditional thin-walled spacecraft tanks, typically designed for 20 bar, become exceptionally robust when used with butane, resulting in significant safety margins
- The system's thrusters can be designed to operate at a practical chamber pressure of 2 bar, eliminating the need for a complex regulation system and reducing the number of costly valves

However, a drawback of using butane is that this kind of propellant must be expelled in its gaseous form, indeed, if liquid-phase butane is expelled, the specific impulse of the thruster decreases dramatically. Therefore, a resistojet is necessary to ensure only vapour-phase butane is vented. Lastly, butane's low freezing point of -138°C makes it an appealing option for missions like GIOVE-A, where thermal control is a critical factor.

5 Reverse sizing

The following data were used to perform the reverse sizing of GIOVE-A satellite's propulsion system:

Performance Parameters			Tank Parameters	
Isp	80s		P_{tank}	0.4 MPa
DeltaV	87.61 m/s (from MA)		T_{tank}	313.15 K
Dry mass	552 kg (total dry mass at launch)		ρ_{tank}	2780 kg/m ³ (titanium Ti6A14V)
ρ_{prop}	$0.53 \times 10^3 \text{ kg/m}^3$ (density of liquid butane at 4 bar)		σ_{tank}	950 MPa (titanium Ti6A14V)
$Mass_{thruster}$	0.05 kg		$R_{specific}$	143.05 J/kg K

Table 8 : Performance and Tank Parameters

5.1 Results

Propellant	Pressurant		Tank	
$Delta V_{real}$	91.99 m/s	V_{gas_i}	V_{tanl_real}	0.0965 m^3
MR	1.1244	M_{gas_i}	r_{tank}	0.2845 m
M_0	620.6475 kg	B	t_{tank}	$3.2941 \times 10^{-4} \text{ m}$
M_{prop_real}	72.4231 kg		M_{tank}	0.9325 kg
V_{prop_real}	0.075 m ³			

Table 9 : Results

So, the total mass budget of the propulsion system is:

$$M_{ps} = 1.1 * (10 * M_{thruster} + 2 * M_{Tank}) = 2.6015kg$$

In which a 10% margin is included to account for cables. Concerning the power budget, the following elements were considered for the computation:

- A maximum of three out of ten thrusters can operate at the same time. The heater power for each thruster is 15W
- The solenoid valves used on the GIOVE-A propulsion system are the modified MV602 supplied by Marotta UK coming from the SSTL'S DCM flight heritage. Considering the valves position as shown in figure 4 and the functioning of Propulsion controller system explained in section 3.4, a total of up to eight valves can operate simultaneously. The power assumed is 1.6 W to which a margin of 10% is added since they are off-the-shelf products with modifications (MAR-PWR-010)

Therefore, the total power budget is:

$$P_{ps} = 3 * P_{thruster} + 1.1 * (8 * P_{Valve}) = 59.08W$$

During the computations, the following margins were used:

- The ΔV was used considering a margin of 5% (MAR-DV-010)
- To the propellant mass was added a 3% to consider the ullage, 2% for the residuals (according to MAR-MAS-080) and 0.5% for the loading uncertainty
- To the propellant volume a 10% of unusable volume was added (MAS-CP-010)
- To the pressurant mass a 20% margin was added (MAR-MAS-090)
- To the tank volume a 5% margin was added (MAR-EP-040)

5.2 Propellant Selection

Given the low ΔV as well as the high reliability and low-cost requirements, the most optimal propellant choice for the GIOVE-A satellite turned out to be liquid butane. The detailed explanation of the rationale behind this choice has been presented in *section 4.1*.

5.3 Tank Sizing and Positioning

GIOVE-A is equipped with two spherical titanium propellant tanks supplied by PSI US, they are mounted to two diagonal shear walls through equatorial mounting lugs. The sizing of the tanks was done taking into consideration a value of the nominal pressure of 22 bar despite the actual pressure used for the liquid butane system on GIOVE-A was just of 4 bar. The reason behind this choice is linked to the fact that the tanks were not designed for a liquid butane system but rather they were sized for a high-pressure hydrazine system. Considering a pressure of 4 bar would lead us to a thickness value of the tanks not technologically feasible. Of course, this results in having an exceptionally robust tank structure and therefore very high safety factors which are well aligned with the reliability requirement of the mission.

Moreover, the same high reliability requirement justifies the choice of having two identical tanks on-board, each connected to a different regulator and half of the thrusters. This configuration ensures redundancy, in fact, even if one of the two tanks or regulators fails, the other can operate normally ensuring the mission completion.

The two identical tanks are placed symmetrically around one of the principal inertial axes, so that the s/c centre of mass and moments of inertia are easily predictable enabling optimal attitude control and manoeuvring throughout the entire mission.

5.4 Pressurant Selection

The reverse sizing was carried out assuming a blow-down model with a blow-down ratio of 5.5. The pressurant present in the tanks is vapour of the butane itself and this, together with a relatively low tank pressure, is the reason why the value of its mass is negligible in the scope of the total mass budget. Since the butane vapour pressure is a direct function of its temperature, the higher the propellant temperature the higher the propellant tank pressure. However, in the tanks the maximum pressure level that butane can reach is far lower than the system is capable of handling (7 bar with respect to 22 bar). Also, during the in-orbit operations, the data retrieved from the temperature sensors in the feed system showed that the tank would usually operate at around 40°C. Therefore, in our computations the temperature in the tanks was assumed to be constant. In addition to that, we have used the isothermal flow assumption in our computations and modelling since the low ΔV provided by the GIOVE-A propulsion system is characterised by a relatively slow mass flow.

5.5 Thrusters

GIOVE-A is equipped with ten T-15 thrusters designed by SSTL. Each of them weights 50 grams and uses a power of 15W.

Variant	Redundant heater power	Propellant	Thrusters	Typical operation temperature	I_{sp}
T50	50W	Xe, N ₂ , Butane	Qualification Model only	Up to 650°C	Up to 57 s
T30	30W	Xe	10 launched on 10 S/Cs, 2 waiting launch	530°C	48 sec
T15	15W	Butane	19 launched on 10 S/Cs, 4 waiting launch	250 - 350°C	> 100 s

Figure 6 : The variants of SSTLs low cost resistojet^[20]

Each thruster can seamlessly switch between cold gas or hot gas mode:

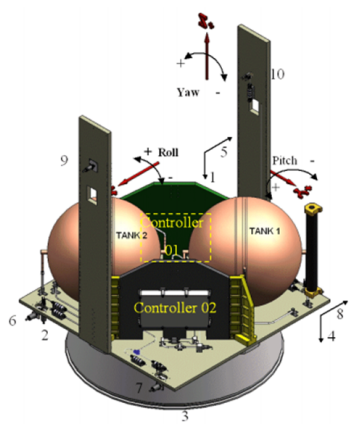
- Cold gas mode – heaters are turned off and the thrust is generated only by the expansion of the pressurised gas, the nominal specific impulse associated with this mode is 60 seconds and is suited for precise manoeuvres
- Hot gas mode – heaters are turned on and the thrust is generated by the expansion of the hot gas, the nominal specific impulse associated with this mode is 80 seconds and is suited for larger manoeuvres

The integrated heaters (main and redundant) are used to increase the Isp performance achieved from the liquefied gas cold propulsion system, and make sure that no liquid phase butane is expelled through nozzle.

The thrusters are positioned symmetrically to provide straightforward and complete control of the spacecraft, as shown in figure 5 there are:

- 4 thrusters on the Z- face (1-4)
- 2 thrusters on the lower part of the X- face (5,8) and X+ face (6,7)
- A single thruster on the upper central part of the X- (10) and X+ (9) faces

Figure 7 : ΔV bar-diagram



TELEMETRY AND TELECOMMAND SUBSYSTEM

1 TMTA Architecture

The Telemetry, Tracking and Command or Communication subsystem provide the interface and the bidirectional communication between the spacecraft and the ground segment, ensuring the reliable transfer of data and remote control of onboard functions. This system represents a part of the control and monitoring architecture of satellites and plays a crucial role in ensuring the operational efficiency and safety of space missions. The aims are to explore the crucial role of data and command management in the context of the TMTA subsystem, through a detailed analysis of current technologies and methodologies applied on the satellite GIOVE-A^[7].

1.1 Space Segment

The space segment of a satellite mission embodies the crucial infrastructure situated in space. It serves as the central hub for transmitting telemetry data, receiving commands from ground stations, and executing control functions essential for the satellite's operation and mission objectives. It is designed to ensure seamless communication, precise tracking, and effective control, thus allowing the satellite's mission success in orbit^[13].

1.1.1 PLATFORM S-band TT&C (SSTL)

The main features are the S-Band Patch Antennas which provide support for communication with the ground segment. This kind of antennas are common for telemetry and telecommand for Earth observation and Space Science missions like GIOVE-A. It produces a hemispherical pattern, and they are positioned for full 4π coverage, which is useful for multiple reasons:

- GIOVE-A can establish communication links with ground stations located in different positions and directions around the Earth, avoiding the need for precise pointing mechanisms;
- it grants high reliability and redundancy; in case of any uneven movement or change in orientation, hemispherical antenna always guarantees a communication link available;
- this kind of antennas are simpler to design and construct than directional ones.

As shown in Figure 1, at the centre of TMTA system scheme, there are the S-Band Uplink Receiver^[22] and the S-Band Downlink Transmitter^[23]. S-Band Uplink Receiver manages low data rate for telemetry and telecommand. GIOVE-A is embedded with a CAN (Controlled Area Network) bus, a communication protocol with the on-board data handling system. So, nominally, received signal are sent to the OBC (on-board computer). Since CAN bus links different subsystem to communicate each other, a CAN Command Decoder is implemented: this enables CAN commands to be directly translated and sent to the subsystem, bypassing the OBC if required. This option is important for an efficient communication between ground and space, especially for telecommand messages. S-Band Downlink Transmitter provide flexible high-speed downlink signals. As for the receiver, this device is characterized by:

- direct link with the OBC;
- CAN bus connection to allow OBC control of transmitter;
- CAN bus connection to let the transmitter take telemetry data directly from other subsystems (crucial part if OBC is not correctly operating).

1.1.2 NAVANT

The NAVANT is an important antenna on board GIOVE-A, part of the payload and not of the TMTA subsystem. Its main role is to transmit a focused signal with constant power in the desired direction, providing an isoflow model. It is capable of operating over a wide range of frequencies, covering the operational spectrum of GIOVE-A. To ensure compliance with the ITU requirements for the storage of radio frequencies of the Galileo programme, an MFUU is used to ensure an output power of about 50 W in the L-band.

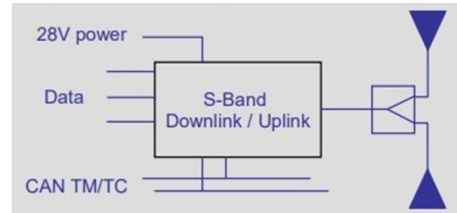


Figure 8 : TMTA Architecture^[21]

1.2 Ground Segment

The Ground Segment acts as an intermediary between satellites in space and ground control. It consists of a sophisticated infrastructure of ground stations, control centers, data processing systems and communication networks, working synergistically to facilitate the effective management of space missions. Since 2003, two years before the launch of the GIOVE-A satellite, the second phase of the Galileo System Test Bed (GSTB-V2) project has been underway. This project serves as a test and validation system for the operational capabilities of the European Galileo satellite navigation system. It constitutes a test environment that faithfully replicates the functionalities and characteristics of the Galileo system. This replication allows engineers to conduct simulations of real operations and evaluate system performance. Infrastructures communicate with each other through a precise public internet-based communication network, using direct links, VPN connections or servers with controlled access for downloading data and parameters directly from the satellite^[24].

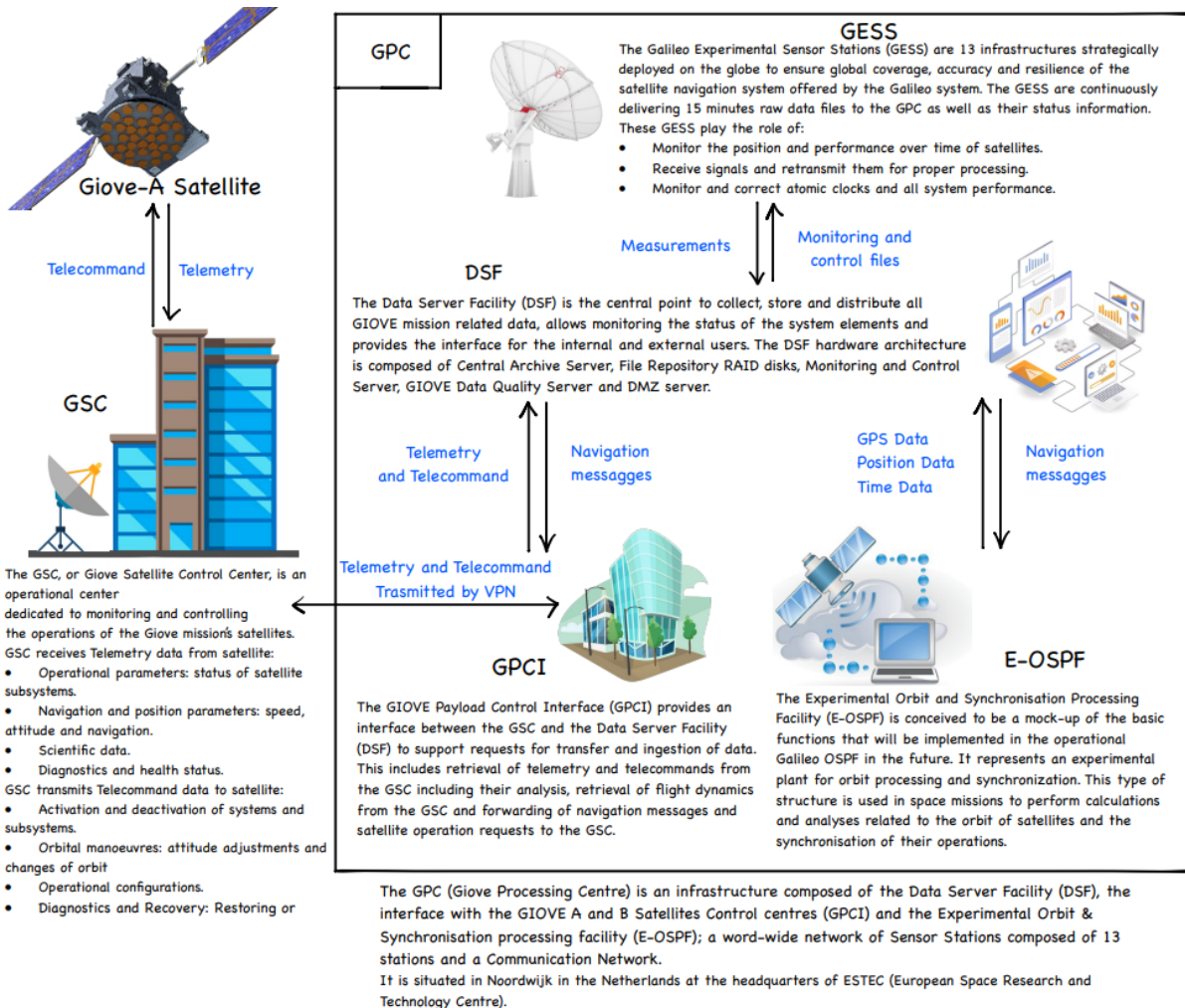


Figure 9 : Ground Segment Architecture

1.3 Phase/ConOps and TMTC Subsystems

Phase/ConOps	TMTC Subsystem
LEOP	<ul style="list-style-type: none"> • Primary goal is successful signal acquisition and tracking, achieved through the RAL 12m antenna, with the SSTL 3.7m antenna providing redundancy to ensure robust communication. • S-band Patch Antennas are crucial, offering hemispherical coverage that enabled link maintenance without the need for precise pointing mechanisms. • The uplink receiver managed telecommands at a low data rate. • Direct link with the OBC and CAN bus connections for control and data retrieval ensures real-time command and control operations

IOT	<ul style="list-style-type: none"> • TT&C is central here to activate and test the payload, with increased data volumes being transmitted. • Ground segment integration with facilities like the Chilbolton Observatory allows for the verification of CW power and modulated spectra, essential for the satellite's operational validation. • High-speed downlink transmitters enables the return of telemetry data to ground stations, underscoring the system's capability to handle large volumes of data securely and efficiently.
Routine Operation	<ul style="list-style-type: none"> • Routine operations benefited from the semi-automated link from the GIOVE Processing Centre (GPC) to the Operations Control Centre (OCC), with telemetry data handled via secure internet links. • Periodic health and status checks were conducted, which involved downlinking telemetry data to monitor the spacecraft's subsystems' performance. • Uplink receiver executes operational telecommands, including adjustments to the satellite's orbit and attitude, system configurations, and payload operations. • Data volume transfer involves consistent but not high-volume data streams, mainly encompassing operational telemetry and occasional payload data dumps. • In case of any onboard anomalies, the TT&C system implements contingency plans, which might include switching to backup systems or modifying operational parameters to stabilize the spacecraft.
EOL	<ul style="list-style-type: none"> • T&C takes charge of executing change orbit maneuvers, managing the precise command sequences necessary for satellite repositioning. • This phase involves a decrease in data volume but an increase in the importance of data precision. • Continuous health monitoring of the satellite's systems ensures a controlled deactivation process. • TT&C system showcases adaptability to varied data requirements and maintained reliable communication links (evident from the minimal data necessary during LEOP to the extensive streams during IOT and critical command communications at EOL).

Table 10 : Phase/ConOps and TMTC subsystems^{[25][26]}

2 TMTC Reverse Sizing

The reverse sizing has been carried out both on the uplink and downlink transmissions of GIOVE-A satellite's TMTC subsystem.

2.1 Downlink

The following data, retrieved from the appropriate datasheet, about the downlink transmitter present on GIOVE-A have been used:

DLINK TRANSMITTER					
Frequency selection	Datarate	Band	Ecoding	Modulation	RF output power
2.2 to 2.3 GHz	9.6 kbps to 8 Mbps	S-band	Convolutional	QPSK	4W

Table 11 : Downlink input data

More precisely, a frequency of 2.3 GHz has been used for the computation in order to size the worst case scenario, indeed, the higher the frequencies the higher the losses.

Regarding the encoding, it is better to choose a convolutional type of coding scheme instead of a block one because it allows to reduce the Error per bit to Noise density.

QPSK modulation is usually preferred when high bit rates and speed transfer of data are required while BPSK modulation is preferred for small amounts of transmitting energy. Since the downlink requires a bigger amount of data to be transmitted, QPSK has been chosen.

In this case, the RF output power is automatically retrieved from the datasheet of the SSTL downlink transmitter. Lastly, The BER is assumed to be 10^{-5} because we are dealing with data downlink and the cable loss is assumed to be equal to -3 db, which is the worst value in order to be conservative.

2.2 Uplink

The following data, retrieved from the appropriate datasheet, about the uplink receiver present on GIOVE-A have been used:

UPLINK RECIEVER				
Frequency selection	Datarate	Band	Encoding	Modulation
2025 to 2100 MHz	9.6 to 19.2 kbps	S-band	Convolutional	BPSK

Table 12 : Uplink input data

In this case the frequency selected for the computation is 2100 MHz while the value of the data rate is 19.2 Kbps. These values have been chosen in order to size the worst case scenario. The BER, instead, is assumed to be 10^{-7} since we are dealing with uplink data and the cable loss is assumed to be equal to -3 db for the same reason of the downlink case. Moreover, in reality, the uplink is un-encoded but to make easier calculation, a convolutional encoding has been assumed.

2.3 Results

Downlink transmitter		Downlink receiver		Losses	
$R_{data,real}$	4 Mbps	$G_r x$	53.0 db	L_{space}	187 db
G_{ant}	2.925 db	$\theta_r x$	19,51°	L_{point}	0.0003 db
$EIRP$	5.95 db	P_{rx}	1.398×10^{-13}	L_{atm}	0.035 db

Table 13 : Downlink results

Uplink receiver		Uplink transmitter		Losses	
$R_{data,real}$	38.4 Kbps	G_{ant}	52.25 db	L_{space}	186 db
G_{rx}	2.18 db	$EIRP$	70 db	L_{point}	2.85×10^{-9} db
θ_{rx}	32.19°			L_{atm}	0.035 db
P_{rx}	3.96×10^{-12} W				

Table 14 : Uplink results

As expected, for the uplink the data rate is considerably lower than for the downlink. This is because, while in the downlink the satellite needs to provide telemetry data and functionalities status of all subsystems and payload equipment, in the uplink only telecommand is transmitted.

The space losses are the main loss contribution. To evaluate them, the highest communication distance between satellite and ground station has been considered to account for the worst case scenario. The atmosphere losses have been retrieved from graphs, knowing the operating frequency of the transmitter and receiver. At this frequency, the rain attenuation is negligible, hence the atmospheric losses comprehend only the Zenith attenuation.

To evaluate the antenna misalignment (de-pointing) loss, it has been modelled as function of the pointing error and the beamwidth of the antenna. The pointing loss increases with the pointing error angle and decreases with the receiver antenna beamwidth.

Lastly, the maximum datarate that the GIOVE-A on-board antennas can handle is 4 Mbps, therefore in the range available from the SSTL downlink transmitter, 4 Mbps has been selected to perform the sizing.

The minimum value of the carrier Signal to Noise ratio considered to compute its margin is 20 db, which is the minimum recommended to have a good signal clarity for non-DSN Earth satellites [12]. However, as shown in the table below, from our computations the obtained margin is not enough to grant clear trackability of the satellite. Of course, for the real mission it is not the case and this discrepancy could be related to models and data assumptions we used in absence of precise data. On the other hand, the computed Error per Bit to Noise density satisfies the inequality thus granting the receiver capability to translate the signal, distinguishing it from the noise.

		Downlink	Uplink
The Error per bit to Noise density	The N_0 has been computed considering a $T_s=253$ K (from the datasheet), therefore $N_0 = -204.6$ db in both cases	The $E_b/N_0 = 10.05$ db. Comparing this value to the minimum, the inequality is respected: $E_b/N_0 > (E_b/N_0)_{min} + 3db$ where $(E_b/N_0)_{min} = 4.2$ db.	In this case the $E_b/N_0 = 44.76$ db. Once again the inequality is respected because the $(E_b/N_0)_{min} = 5.1$ db.
Modulation index reduction	The modulation index, in both cases, was assumed to be 78°	Carrier modulation index reduction is equal to $P_{mod,loss} = -13.64$ db and the complete carrier power $P_{carrier} = -142$ db.	$P_{mod,loss} = -13.64$ db, $P_{carrier} = -127.66$ db.
Signal to Noise Ratio	Both receivers have a bandwidth of 4 MHz and the $SNR_{min} = 20$ db.	The signal to noise ratio is computed as: $SNR_{carrier} = -3.58$ db. Therefore the margin is $SNR_{margin} = -23.584$ db.	In this case $SNR_{carrier} = 10.94$ db $SNR_{margin} = -9.05$ db

GROUND STATION SELECTION: The GIOVE-A satellite control center is based at SSTL in Chilbolton (making use of existing facilities), with ground stations at RAL and in Kuala Lumpur, Malaysia. The Chilbolton base is a Space Monitoring Facility provided with a 25m parabolic antenna to track and characterize Earth orbiting satellites. It is the most important ground station for the mission, since it performed the IOT of ESA's GIOVE-A spacecraft. Additionally, it had a dual function of uplink transmitter and downlink receiver, therefore this ground station has been chosen for the current computation.



Figure 10 : S-patch antenna^[21]

ANTENNA SELECTION: On the GIOVE-A satellite there are two S-Band Patch antennas built by SSTL. One is used as transmitter for telemetry downlink, while the other as receiver for telecommand uplink.

To compute the gain of the Patch antennas the formula for the planar array has been used since they belong to that category with a $\lambda=0.1303$ m. For the uplink, instead, the gain of the transmitter antenna, the one on ground, has been computed from the formula for parabolic antennas. For the uplink receiver the formula is the same of the downlink since it's the same S-band patch antenna but with a $\lambda=0.1421$ m^[27].

AMPLIFIER SELECTION: The S-band High Power Amplifier onboard GIOVE-A, manufactured by SSTL, serves both uplink and downlink functions. A high RF output power is essential for maintaining adequate SNR at the receiver. Solid-state power amplifiers are preferred in such scenarios due to their longevity and reliability. Compared to traditional TWTA amplifiers, solid-state amplifiers offer prolonged lifespan, ensuring consistent performance without frequent maintenance. Additionally, they contribute to more compact and lightweight satellite designs.

CONTACT STRATEGY: Throughout the whole GIOVE-A mission, the satellite has had contact with 11 to 17 different active ground stations making the average visibility time of the spacecraft close to 85% of the orbital period. Additionally, being GIOVE-A a MEO orbiter, its typical communication window for each ground station in visibility range is relatively long (about 1 hour, compared to few minutes for LEO satellites). For these reasons, plus the relatively low data volume for telemetry, maintenance and telecommand (69 Mbit for uplink and 14.4 Gbit for downlink maximum), the data rates managed by the TMTC subsystem are in line with similar Earth observation missions for the same functions, without any particular requirement.

POSITIONING OF ANTENNAS: The RF subsystem has SSTL S-band receivers and transmitters which provide a full 4π coverage. It boasts full redundancy, enabling direct commanding of connected equipment via the CAN bus. The dual antennas are configured in a +Z -Z arrangement, with the -Z antenna Nadir pointing. Due to their hemispherical patterns, offering omni-directional coverage, their placement on the satellite is a non-critical aspect^[28].

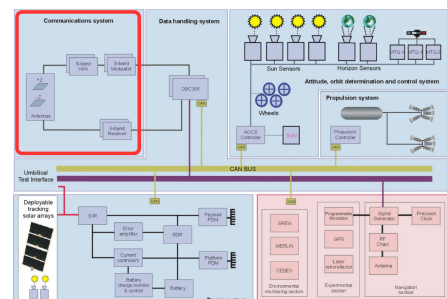


Figure 11 : TMTC architecture^[26]

ATTITUDE AND ORBIT CONTROL SUBSYSTEM

1 AOCS architecture

The AOCS subsystem is designed to ensure full control of the satellite throughout its entire operational lifetime and to enable the achievement of the mission's primary objectives. GIOVE-A's AOCS interface modules operate 6 gyros, 16 sun sensors, 2 Earth horizon sensors, 4 reaction wheels, 3 magnetorquers and 10 thrusters[1]. It is highly redundant, so it is able to grant both Nominal Operational Mode and the Attitude Safe Mode.

1.1 Sensors

Earth Horizon Sensor (EHS): the Infrared Earth Sensor (IRES) is a two-axis scanning sensor designed for Pitch and Roll attitude angles measurements relative to the Earth's center. Operative in both GEO and MEO, assisting in spacecraft stabilization during orbit operations. The sensor uses infrared radiation modulation within the 14-16.25 μm band: Earth's horizon detection through electro-mechanical means. The single telescope and mirror design generate Earth/Space and Space/Earth pulses along a 45° Earth latitude scan path.^[29]

Sun Sensor (SSN): the 2-axis DMC Sun Sensor provides accurate measurements of Sun angles with a ± 50 degree field of view along two orthogonal axes. The sensor outputs two analog signals per axis, which are combined and linearized to determine the relevant angles.^[30]

Gyroscopes: the QRS11 Quartz MEMS Angular Rate Sensor is a compact, reliable gyroscopic sensor utilizing MEMS technology. It provides stability and long-term performance without any moving parts, making it suitable for prolonged missions in space.^[31]

Parameter	Value
Earth Horizon Sensor (EHS)	
Output data rate	10 Hz
Random error	< 0.05° (3σ)
Bias error	< 0.02°
Power consumption	< 4 W
Mass	< 2.5 kg
Sun Sensor (SSN)	
Mass	0.3 kg
Mass consumption (sunlit)	< 100 mW
Power consumption (dark)	< 10 mW
Accuracy	1.0° (95%)
Radiation tollerance	up to 5 kRad (Si)
Gyroscopes	
Full-scale range	$\pm 100^\circ/\text{s}$
Rate measurement noise ARW	< 0.6°/s/ $\sqrt{\text{Hz}}$
Maximum bias	0.5°/s
Steady-state bias instability RRW	216°/hr/ $\sqrt{\text{hr}}$

Table 15 : Detailed specifications of sensors^{[29][30][31]}

1.2 Actuators

Reaction Wheels (RW): GIOVE-A is equipped with four 200SP Smallsat wheels to grant precise 3-axis control. The 4 wheels are mounted inside the main body of the satellite in a pyramidal configuration.^[32]

Magnetorquers (MTQ): three dual-core magnetorquers MTR-30 are mounted on-board to ensure reliable attitude control and for RW desaturation purposes.^[33]

Thrusters: the spacecraft is equipped with ten butane-based SSTL T-15 low power resistojets, designed for orbit correction, station-keeping, and desaturation (low cost maneuvres)^[34]. They can be used as resistojets for demanding Δv maneuvers by heating the propellant in a gaseous state or in a cold gas mode for precise control through small thrust impulses. In the following *Table* a summary of the attitude control operations, and their relative Δv budget, for the whole mission is presented:

Attitude Manoeuvre	Delta V requirement [m/s]	Performance Provided
Yaw rotation	9.54	APE
Momentum off loading	0.20	Duration Budget
Attitude Control during LEOP	0.21	Duration Budget
Attitude Control in RCS mode	1.44	Duration Budget
ESRs	2.22	Orbit Correction Budget

Table 16 : Attitude control delta V Requirements^[35]

Yaw rotation is essential to correctly orient the spacecraft, so it refers to the absolute attitude pointing budgets. On the other hand, manoeuvres linked to duration budget are the ones which ensure the overall duration of the mission. Lastly, the orbit correction budget is crucial for managing the spacecraft's relative orientation to external factors like radiations.

Parameter	Reaction Wheels (RW)	Parameter	Magnetotorques (MTQ)
Mass	5.2 kg	Mass	1.8 kg
Volume	$\varnothing 240 \times 90$ mm	Dimensions	378 x 74 x 49 mm
Max. Torque	0.240 Nm	Power Consumption	1 W at 5 V
Max. Speed	± 5000 rpm	Magnetic Moment (single coil)	± 30 Am ²
Ang. Momentum	12 Nm	Magnetic Moment (dual coil)	± 45 Am ²
Power Cons (standby)	3.3 W	Scale Factor	0.15 Am ² /mA
Power Cons (5000 rpm)	16.3 W	Linearity	$\pm 5\%$ over ± 30 Am ²
Power Cons (max tq)	145 W	Residual Momentum	< 0.1 Am ²
Parameter	Thrusters		
Mass	15 g		
Power Cons	30 W		
Thrust	up to 100 mN		
Specific Impulse	about 80s		
Operation Temp	about 250°C		

Table 17 : Specifications of the actuators^{[32][33][34]}

Solar Array Drive Mechanism (SADM): for a comprehensive analysis, it is considered this further non-traditional actuator, since the AOCS is responsible for its operations, aiming to re-orient the solar arrays depending on the mission phases.

1.3 AOCS Rationality

As suggested by the high and multiple pointing requirements, that are granted by the selected sensors, the architecture of AOCS is 3-axis control. Moreover, the information of Earth and Sun relative positions hints that the AOCS nominal operation aims to: The antenna boresight is maintained in nadir pointing alignment with the Z-axis (see Figure 1) to ensure reliable communication with ground stations, maintaining a maximum error of 0.55° (σ). The Solar Arrays are continuously oriented towards the Sun (see Figure 1) to sustain optimal power supply to the spacecraft and its payload, with a maximum error tolerance of 2.1° (3 σ). The +X face of the satellite remains pointed towards deep space (see Figure 1) to manage thermal conditions effectively.

As notable in Figure 1, the attitude control keeps the spacecraft-Sun vector nominally in X-Z body plane; due to the Nadir pointing the rotation of solar array (to maintain normal solar incidence) is constrained to be about Y axis, so a continuous Yaw manoeuvre around the orbit is performed. Whilst Earth position is continuously given by horizon sensor, for the Sun it is important to consider the eclipse problem: in this condition, there is a lack of information for periods of up to approximately a quarter of orbit. To overcome this problem, it is implemented an approach based on momentum bias to provide short term stability against disturbance torques. Notice that gyros are not used because they would lead to an unacceptable error of 10° for Yaw measurement (far from objective in Table 2). Instead, it is estimated a Yaw measurement through the available info of Pitch and Roll axis, and wheel speed measurement, under the assumption of conservation of the angular momentum of the system. This method is not the simplest possible, but it ignores the environmental disturbances, and it is less sensitive to pointing errors, minimizing the risk. To implement this strategy, it is necessary to maintain the total angular momentum of the system perpendicular to the orbit plane: a feed forward momentum profile is introduced to force the spacecraft to follow the required Yaw steering requirement. Momentum Bias is a common and cheap solution for long missions as GIOVE-A. Another issue is the singularity when the angle between Earth-Sun vector and the orbital plane is 0° (β in Figure 1). Approaching this limit, the demanded rates and accelerations will be high enough to cause a Yaw momentum needed larger than the actuation torque available. To avoid singular configuration a threshold on β is set, β_{critc} , and whenever $\beta < \beta_{critc}$, an adjust profile is adopted: the primary goal of the modified profile is to decrease the necessary Yaw rate during the Yaw flip manoeuvre. This

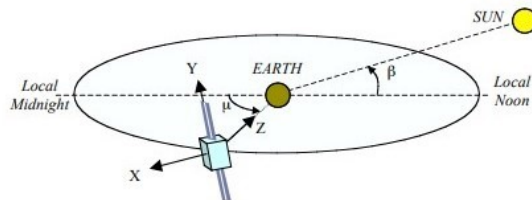


Figure 12: Nominal Pointing Scheme^[36]

is achieved through a 'bang-coast-bang' torque profile, where the Yaw rate increases steadily under constant acceleration, then remains constant for a period if needed, and finally decelerates. The profile is engineered to ensure that the Yaw angle and rate at the beginning and end of the adjusted section match those of the original path^[36].

2 AOCS Sizing

2.1 Pointing Budgets Inputs for Each Subsystem

In the process of designing the AOCS subsystem, it is essential to identify the various mission modes for each phase and develop an input pointing budget that considers the pointing requirements of all subsystems.

Stand-by Mode: the satellite is not actively engaged in its primary mission operations but remains in a state that allows for quick reactivation. Key features of the stand-by mode include: pointing solar panels towards the Sun and pointing antennas towards Ground Station.

Safe Hold Mode: it is a special state that the satellite enters either upon manual command from the ground or autonomously when it detects a potential hazardous condition. In this mode, all payloads and non-essential systems are powered down, ensuring the solar arrays remain pointed at the Sun, maintaining attitude control, and sustaining communication with the ground station.

Normal Mode: the satellite performs its primary mission functions; these include: full Payload Operation, regular communication with GS, attitude and orbit control, power management and thermal control. Therefore, the Normal Mode is comprehensive of the Communication Mode and the Power Generation Mode, hence only the Normal Mode is shown in the table.

Orbit Control Mode: it includes activities related to maintaining and adjusting the satellite's orbit and attitude. Its key functions are: station-keeping, orbit change, de-tumbling and slew manoeuvres, ground-assisted and thruster-based control.

The following table contains all the pointing indices for each subsystem and for all the mission modes. To fulfill the high pointing accuracy requirements of the GIOVE-A mission, the slew manoeuvre rate was set to a constant value of 0.5°/s. As for the rate and drift budget, the range was set to any attitude within 30° of Nadir with rotational rates below

	Orbit Control Mode	Normal Mode	Stand-By Mode	Safe Hold Mode
TTMTC	APE: 0.55° AKE: 0.3°	APE: 0.55° AKE: 0.3°	APE: 0.55° AKE: 0.3°	APE: 0.55° AKE: 0.3°
PS	APE: 0.01° AKE: 0.005°	APE: 0.02° AKE: 0.01°	APE: 0.02° AKE: 0.01°	APE: 0.02° AKE: 0.01°
EPS	APE: 1.50° AKE: 0.5°	APE: 1.41° AKE: 0.3°	APE: 1.41° AKE: 0.3°	APE: 1.41° AKE: 0.3°
TCS	APE: 0.4° AKE: 0.1°	APE: 0.3° AKE: 0.1°	/	/
AOCS	APE: 0.4° AKE: 0.15°	APE: 0.3° AKE: 0.1°	APE: 0.3° AKE: 0.1°	APE: 0.55° AKE: 0.3°
PL	APE: 0.8° AKE: 0.3°	APE: 0.55° AKE: 0.3°	/	/

Table 18 : Input Pointing Budget^{[37][36]}

The drift was set to 0.01° over 20 minutes to meet the high demanded accuracy^[38].

The Normal Mode generally exhibits higher accuracy across all subsystems, except for the propulsion subsystem whose accuracy is higher in the Orbit Control Mode in order to guarantee a correct accomplishment of the required orbital manoeuvres. The higher accuracy of the Normal Mode is due to the fact that it is crucial for the mission's goals achievement. The telecommunication subsystem presents the same accuracy for both modes since communication with Ground Station is crucial both for the nominal operations and the orbital manoeuvres. In the Safe Hold and Stand-by modes, there are no defined pointing requirements for the Payload because it is deactivated in these modes. Nevertheless, the TTMTC and EPS follow the same stringent pointing requirements as the Orbit Control Mode to comply with mission objectives.

2.2 Attitude Sensors and Actuators Suite Selection According to Mode

Being GIOVE-A a test-bed and a validation mission for the Galileo navigation system, the Normal Mode is crucial since it is the only mode capable of supporting payload operations whose success is crucial to achieve

GIOVE-A's main goals. For these reasons the AOCS design is carried out around this mode's requirements, which were already listed in *paragraph 1*.

GIOVE-A is a planetary mission, therefore two Earth sensors have been selected for Roll and Pitch angle measurements, while sixteen Sun sensors have been chosen, for their high accuracy, to determine the Sun direction vector, crucial for completing the attitude determination. The two Earth sensors were placed on the +Z face of the spacecraft which is Nadir pointing. In order to have a 360° field of view, two Sun sensors were placed on each face of the spacecraft main body. In addition, two Sun sensors were placed on each wing to determine the Sun tracking solar arrays attitude, which is independent from the spacecraft's attitude. This extensive sensor number offers a high level of redundancy, ensuring both safety and the necessary precision for the Normal Mode, which requires the most accurate and complex hardware to ensure the proper conduct of payload operations.

Regarding instead the actuators selection, it is driven by the high precision attitude accuracy standards (0.1°-1°) that can be achieved with three-axis stabilization control. This approach needs the integration of Sun sensors and gyro sensors for precise referencing, together with reaction wheels and thrusters to avoid saturation. Even though the whole design of the AOCS system is based on the Normal Mode, the actuators choice is also driven by the Orbit Control Mode in which the spacecraft performs the initial de-tumbling manoeuvre and the orbit change towards the graveyard orbit. The first manoeuvres during the LEOP phase are fundamental for the beginning of payload commissioning and the IOT phase, hence high accuracy is demanded for the actuators with a required control torque of 16Nm and a thrust > 35mN per each thruster^[39]. More precisely, the thrusters are located on the external faces of the main body as follows: 4 thrusters on the Z- face, 2 thrusters on the lower part of the X- face and X+ face, a single thruster on the upper central part of the X- and X+ faces. This symmetric configuration provides straightforward and complete control of the spacecraft.

2.3 Attitude Sensor Sizing According to Pointing Knowledge Needs

As illustrated in the pointing budget analysis, the mission's high accuracy requirements heavily influenced the sensors selection. In particular, for the attitude control subsystem, precision of 0.3° is mandated for Roll, Pitch, and Yaw measurements. Consequently, Earth horizon sensors have been chosen for their remarkable accuracy (0.05°-1°) and their ability to provide direct Earth-relative data essential for Earth-pointing space crafts^[37]. Additionally, Sun sensors were opted for to enhance the precision of Yaw angle measurements (0.005°-3°). Finally, gyroscopes were included for redundancy.

2.4 Disturbance Effects

To estimate the disturbances that affect the spacecraft, a preliminary analysis on the moments of inertia has been conducted and the assumption of rigid body has been made to simplify the computations. Firstly, the center of mass has been retrieved:

$$\vec{CoM} = [0.65 \quad 0.825 \quad 1.012] m \quad (1)$$

It does not coincide with the geometric center.

This disparity arises when considering that along the Z axis, the center of mass noticeably shifts closer to the -Z face, where the tanks are placed since they considerably outweigh the NAVANT (16kg) situated on the +Z face (Nadir pointing). The configuration of the center of mass is presented in *Figure 2*. So, considering the provided information and defining the center of mass as the origin of the ref. system, the inertia matrix of GIOVE-A is:

$$\mathbf{I} = \begin{bmatrix} 870.23 & 0 & 0 \\ 0 & 236.08 & 0 \\ 0 & 0 & 795.27 \end{bmatrix} kg \cdot m^2 \quad (2)$$

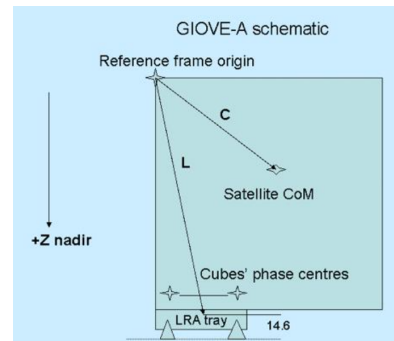


Figure 13 : CoM location^[40]

To perform a more detailed analysis on the external disturbances acting on GIOVE-A, a Simulink model has been used. In the case of GIOVE-A, the main disturbances come from the solar radiation pressure, the gravity gradient and the Earth's magnetic field. The aerodynamic drag is not considered, since it is negligible for orbits above 700 km. Considering a period of one orbit, the maximum values assumed by the environmental disturbance acting on the spacecraft are:

External Disturbances [Nm]		
$T_{SRP} = 3.154 \cdot 10^{-5}$	$T_{GG} = 1.458 \cdot 10^{-5}$	$T_{MAG} = 9.534 \cdot 10^{-8}$

Table 19 : Maximum values of the torques

Therefore, the total torque due to external disturbances is given by: $T_{TOT} = 2 \cdot (T_{SRP} + T_{MM} + T_{MAG}) = 9.2443 \cdot 10^{-5} Nm$ in which a margin of 100% has been introduced.

For a rigid body the torque is expressed as:

$$\vec{T} = \sum_{i=1}^n \vec{r}_i \times \vec{F}_i \quad i = 1, 2, \dots, 10 \quad (3)$$

with r_i being the distance of each surface's pressure center to the CoM and F_i the force depending on the perturbation type. In the case of the Solar Radiation Pressure, the force is computed as^[41]:

$$\vec{F}_i = -PA_i(\hat{S}_B \cdot \hat{N}_{Bi}) \left[(1 - \rho_s)\hat{S}_B + \left(2\rho_s(\hat{S}_B \cdot \hat{N}_{Bi}) + \frac{2}{3}\rho_d \right) \hat{N}_{Bi} \right] \quad (4)$$

In Equation (4) the specular reflection ρ_s is assumed to be 0.6 while the diffusion reflection ρ_d is equal to 0.1. $P = \frac{F_e}{c}$ where F_e is the solar constant ($1367 W/m^2$) for Earth Satellites^[37] and c is the speed of light.

In the computational model, the SRP torque is assumed to give a contribution different from zero only for those surfaces for which $\hat{S}_B \cdot \hat{N}_{Bi} > 0$, namely those ones facing the Sun. More precisely, \hat{N}_{Bi} is fixed in the time instant because the assumption of fixed solar arrays has been made to simplify the simulation process. However, this simplification overlooks the continuous rotation of the GIOVE-A sun-tracking solar arrays, always adjusting to face the Sun. As a result, this computational model may underestimate the global trend of the SRP torque, but not its maximum value linked to the worst case scenario.

Considering instead the Gravity gradient torque, the equation used to implement it is^[41]:

$$\vec{T}_{GG} = \frac{3\mu_E}{R^3} \begin{Bmatrix} (I_z - I_y)c_2c_3 \\ (I_x - I_z)c_1c_3 \\ (I_y - I_x)c_1c_2 \end{Bmatrix} \quad (5)$$

The director cosines $c_{1,2,3}$ have been computed using the Euler equations for the dynamics and Direct cosines matrix (DCM) for the kinematics.

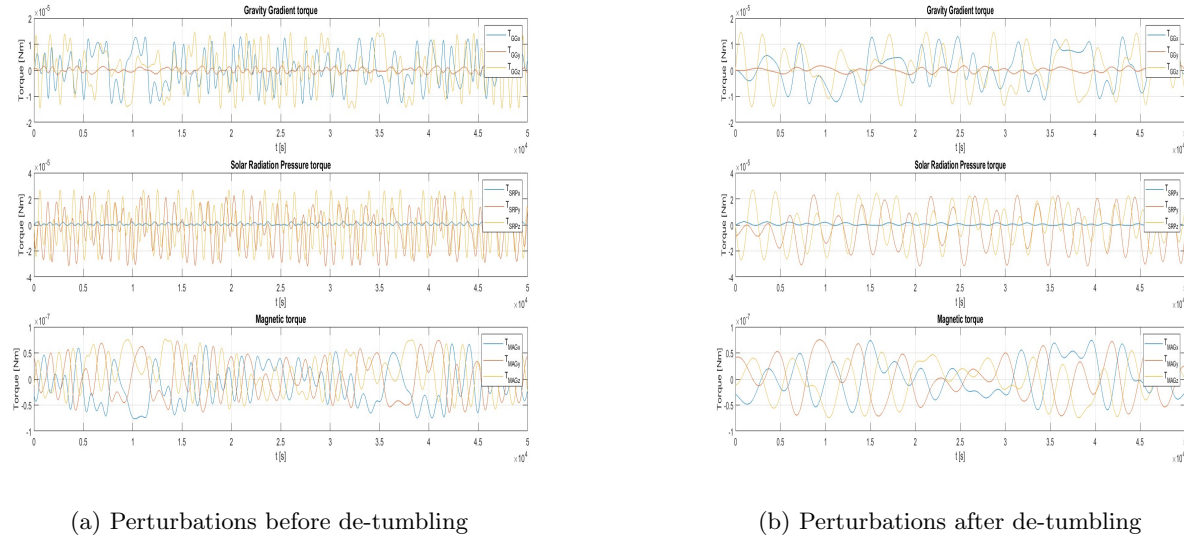
Lastly, to compute the disturbance due to the Earth magnetic field, it has been modelled as a dipole field and its formulation has been retrieved from the literature^[41]. It is a realistic assumption since GIOVE-A orbit is above 7000 km from ground^[41].

So, the equation implemented in the Simulink model is:

$$\vec{M} = \vec{j}_B \times \vec{b}_B \quad (6)$$

where an average constant value, representing a worst case scenario^[41], is assumed for the residual magnetic induction due to currents in the satellite: $\vec{j}_B = [0.1 \quad 0.1 \quad 0.1] A \cdot m^2$

Therefore, an analysis of the temporal evolution of disturbances encountered by GIOVE-A over the duration of one complete orbit ($5.0756 \cdot 10^4$ s) is carried out. Initially, the disturbances are computed assuming a non-zero initial angular velocities, indicative of the satellite's pre-detumbling state. Subsequently, as the orbit progresses and detumbling procedures are executed, an alteration in torque behavior is observed. Initial angular velocities are set to $[0 \ 0 \ n_E]$, where n_E denotes the Earth's rotational speed. GIOVE-A is now de-tumbled and Nadir pointing.



Considering a SRP torque, it is evident that the X component has the lowest values, which aligns with the fact that the +X face is always oriented towards deep space. Conversely, the Z direction shows the highest value: indeed, after detumbling, we aim for the solar arrays to consistently face the Sun, thus the SRP along the Z direction increases since the solar arrays' area is perpendicular to the line connecting the Sun and the spacecraft. This happens in Stand-by and Safe Hold Modes, where the requirement for Sun pointing must be met. The same applies to the Normal mode, during which the Nadir pointing requirement is also met.

2.5 Actuators Sizing

Our simulation revealed a maximum marginalized (+100%) disturbance torque of $9.2 \cdot 10^{-5} Nm$. Starting from this value we have conducted the sizing of the actuators onboard the GIOVE-A satellite, whose numerical results are presented in the following table, in which the white cells represent the inputs while green ones represent the outputs:

Reaction Wheels		Thrusters system		Magnetorquers	
Normal mode		Normal mode		Normal mode	
$h_{rw_{max}}$	12 Nms	n_{th}	5	$T_{mag_{max}}$	$2 \times 10^{-5} Nm$
$h_{rw_{orbit}}$	3.2 Nms	$F_{th_{max}}$	100 mN	$t_{des_{mag}}$	2.3 days
$n_{saturation}$	3.8 orbits	Isp_{th}	90 s		
Orbit Control mode		$F_{th_{dis}}$	$1.6 \times 10^{-5} N$		
θ_{slew}	180 deg	$t_{des_{th}}$	30.5 s		
θ_{rate}	0.5 deg/s	$m_{prop_{des}}$	3.4 g		
$T_{rw_{max}}$	0.24 Nm	$M_{prop_{des}}$	5.07 kg		
t_{min}	360 s	Orbit Control mode			
$T_{rw_{slew}}$	0.09 Nm	θ_{slew}	180 deg		
		θ_{rate}	0.5 deg/s		
		t_{slew}	83.9 s		

Table 20 : Sizing input data and numerical results

2.5.1 Reaction Wheels

Considering the normal mode, given the maximum disturbing torque and the satellite's orbital period, we have evaluated the angular momentum stored by the reaction wheels in one orbit $h_{rw_{orbit}}$. It is recommended that the angular momentum stored in one orbit is less than the maximum angular momentum that the reaction wheels can absorb. This ensures that the desaturation process does not have to occur too frequently. Therefore, the quantitative assessment of the angular momentum absorbed by the wheels is a driving factor in their sizing and selection.

In the case of GIOVE-A, given the specifications (retrieved from the datasheet^[32]) of the actual wheels onboard and the disturbances identified from our simulation, it was found that the wheels saturate every 3.8 orbits. It is a reasonable result assuming that only the reaction wheels are used to counteract the disturbing torque.

Considering, instead, the orbit control mode, we also conducted the sizing of the reaction wheels for the execution of a 180° slew manoeuvre with a worst-case scenario approach. First, we computed the minimum time for the manoeuvre, t_{min} , considering a constant angular rate $\theta_{slew} = 0.5 \text{ deg/s}$. Then, assuming a slew manoeuvre with constant acceleration and braking, the torque $T_{rw_{slew}}$ required from the reaction wheels to perform the manoeuvre was calculated using the following formulas:

$$t_{min} = \frac{\theta_{slew}}{\theta_{rate}} \quad T_{rw_{slew}} = 4\theta_{slew} \frac{I_{max}}{t_{min}^2} \quad (7)$$

To successfully complete the manoeuvre within the given time, the required torque must be less than the maximum torque that the reaction wheels can exert $T_{rw_{max}}$. In the specific case of GIOVE-A, given the above input data and the specifications (retrieved from the datasheet^[32]) of the actuators involved, it was found that the reaction wheels are capable of performing a complete slew manoeuvre of 180° within the given minimum manoeuvre time.

2.5.2 Thrusters System

Starting from the normal mode, for the sizing of the thrusters system, we evaluated firstly the force required from the thruster system $F_{th_{dis}}$ to counteract the external disturbances:

$$F_{th_{dis}} = \frac{T_{dis}}{n_{th} L_{arm}} = 1.6 \times 10^{-5} \text{ N} \quad (8)$$

For the orbit control mode, we computed the minimum time t_{slew} required to execute a 180° slew maneuver utilizing a no-coasting model that includes only acceleration and braking. This calculation considered the maximum thrust $T_{th_{max}}$ obtained from the datasheet^[34], the simultaneous activation of five thrusters, which is the maximum possible for the GIOVE-A propulsion system.

$$t_{slew_{th}} = \sqrt{\frac{\theta_{slew} I_{max}}{n_{th} F_{th_{max}} L_{arm}}} = 83.9 \text{ s} \quad (9)$$

Moreover, the thrusters can be employed for the desaturation of the reaction wheels. By considering the maximum angular momentum stored by the wheels $h_{rw_{max}}$ and the maximum torque exerted by the thrusters $T_{th_{max}}$, we computed the desaturation time $t_{des_{th}}$, assuming this operation is performed solely by the thrusters:

$$t_{des_{th}} = \frac{h_{max_{rw}}}{n_{th} L_{arm} F_{th_{max}}} = 30.5 \text{ s} \quad (10)$$

Knowing the time necessary to complete the desaturation of the wheels, the available thrust, and the specific impulse of the propulsion system $I_{sp_{th}}$ (as retrieved from the datasheet^[34]), we were able to compute the mass of propellant needed to complete the desaturation of one wheel for one time:

$$m_{prop_{des}} = \frac{t_{des_{th}} F_{th_{max}}}{I_{sp} g_0} = 3.4 \text{ g} \quad (11)$$

Finally, by estimating how frequently the desaturation needs to occur, the duration of the mission, and the number of wheels to desaturate, we computed the total mass of propellant needed for the desaturation process throughout the entire mission $M_{prop_{des}} = 5.07 \text{ kg}$. It is important to note that this mass is overestimated due to the assumption that only the thrusters are used for the desaturation, while in the actual mission, magnetorquers are also used for this purpose to optimize fuel consumption.

Additionally, following a similar approach to the computation of the propellant needed for the desaturation process, we have also estimated the mass of propellant needed for the station keeping of the satellite throughout the entire nominal mission: $m_{prop_{sk}} = 1.3 \text{ kg}$.

Finally, we evaluated the mass of propellant needed for the execution of one slew manoeuvre of 180° performed in the minimum time computed before:

$$m_{prop_{slew}} = \frac{2F_{th_{max}} t_{slew}}{I_{sp} g_0} = 19 \text{ g} \quad (12)$$

2.5.3 Magnetorquers

GIOVE-A is equipped with three magnetorquers, mounted along the three principal axes. This configuration enables the generation of a total torque in any given direction. However, the maximum torque that these actuators can provide is significantly smaller compared to the capabilities of the reaction wheels and thrusters. As a result, the primary function of the magnetorquers is to steadily desaturate the onboard wheels.

In the context of sizing this actuator, we have estimated the desaturation time of the wheels, t_{des_mag} , following a similar procedure and equation used for the thrusters sizing, assuming that only magnetorquers are utilized for this function. This computation was conducted by considering the maximum angular momentum stored within the wheels $h_{rw_{max}}$ and the maximum available torque provided by the magnetorquers $T_{mag_{max}}$, as retrieved from their datasheet^[33].

2.6 Mass and Power Budget

The mass and power budgets for all elements of the AOCS subsystem in the worst-case scenario, where all units are active and consuming maximum power, are summarized in the following table. The necessary data for these estimations have been obtained from the datasheets of the actual components onboard GIOVE-A.^{[32][34][33][30][29][42]}

As evident from the table, the reaction wheels contribute the most to both the mass and power budgets. While the mass value is reasonable and compliant with the real mission, the power value is significantly overestimated. This overestimation arises from considering the worst possible case scenario, where all four wheels are spinning simultaneously at maximum speed, which is a very unlikely situation to occur during the operational life of the satellite.

The second largest contribution to the power budget comes from the thrusters. This is because they are equipped with resistive heaters, which activate only when the thrusters are not operated in their nominal cold gas mode.

	Mass Budget	Power Budget
Reaction wheels	20.8 kg	580 W
Thrusters	0.54 kg	90 W
Magnetorquers	5.4 kg	3 W
Sun Sensor	4.8 kg	1.6 W
Horizon Sensor	5 kg	8 W
SADM	6 kg	6 W
Total	42.54 kg	688.6 W
Total Marginalised [20 %]	51.05 kg	826.32 W

Table 21 : AOCS Mass and Power Budget

THERMAL CONTROL SUBSYSTEM

1 TCS Subsystem

The thermal control subsystem of a satellite is a crucial part for regulating internal temperatures and ensuring optimal performance in the extreme conditions of space. It employs a combination of passive and active techniques to manage heat generated by onboard systems, dissipate excess heat into space, and prevent temperature fluctuations that could impact sensitive components.

The temperature inside the satellite is therefore maintained within the preset operating ranges if and only if all heat sources, both external and internal, are perfectly controlled, as shown in *Figure 1*:

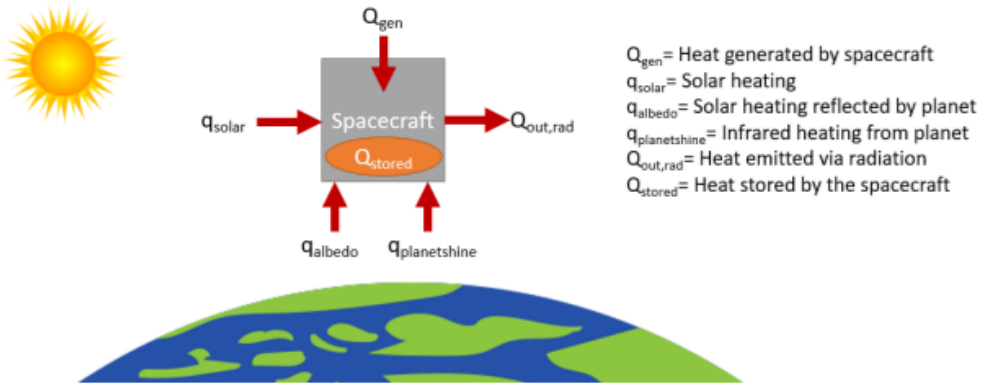


Figure 14 : Orbiting spacecraft heating simplified overview^[43]

1.1 TCS Architecture

GIOVE-A TCS' architecture mostly regards passive control, usually preferred for its simplicity, reliability and cost-effectiveness. However, for most critical situations, active thermal control is adopted as well. In the following subsections a brief presentation is reported, with a deeper analysis in subsections 2.3.1 and 2.3.2.

1.1.1 Passive Thermal Control

Passive thermal management of GIOVE-A is predominantly achieved through the use of **radiators**. These radiators play a crucial role in maintaining safe temperature levels, especially for sensitive payloads like the RAFTS. Solar arrays, which have high emissivity and absorptivity, also function as radiators, dissipating surplus heat. These solar cells are mounted on deployable panels that are thermally isolated from the main structure of the spacecraft. During launch, these panels remain closed, shielding the main spacecraft bus and thereby reducing heat accumulation during this phase. For what concern the **coating**, the exterior of GIOVE-A is coated in black paint, to absorb sunlight and radiate excess heat. The aim is to ensure a stable satellite temperature, avoiding overheating of on-board instruments. To enhance thermal conductivity, **doublers** are used to fill voids within the spacecraft. Thermal doublers are employed to improve conduction and spread the heat across the in-plane thermal conductivity of the material.

Multi-Layer Insulation (MLI), or thermal blankets, are essential for insulating the spacecraft's surfaces. MLI reflects and blocks thermal energy from both the spacecraft and the external environment, minimizing heat emission. Comprising several layers that do not directly touch each other, MLI offers superior insulation properties.^[37]

1.1.2 Active Thermal Control

GIOVE-A utilizes **heaters** to actively manage the temperature of critical components, ensuring they remain within designated operational ranges. This thermal regulation is controlled by the Thermal Management Unit (TMU), which continuously monitors component temperatures using sensors, particularly thermocouples, placed strategically across various surfaces.^[37]

1.2 Thermal Environment

1.2.1 Thermal Flux Consideration

During launch and early orbit, the spacecraft encounters variable external thermal conditions as it exits Earth's atmosphere. Passive thermal absorption method is applied on the Y radiators for cases when spacecraft systems are unpowered and particularly susceptible to temperature extremes – this is important for stabilizing the thermal environment until the spacecraft's active systems can take over. The solar arrays dissipate excess heat into the external environment and the solar cells are placed on the deployable panels for their high emissivity and absorbtivity, thermally isolated. During launch, they are closed since they serve as the protection for the main spacecraft bus - which reduces heat buildup. During operation, the spacecraft is continuously exposed to:

- Direct sunlight: the solar flux intensity follows an inverse square law with distance from the Sun. It varies with the spacecraft's location, and the reference temperature is based on the assumption that the planet behaves as a black body ($\epsilon = 1$). Typically, the solar flux is approximated as 1367.5 W/m^2 for a reference sphere, providing a general indication of the local thermal environment;^[37]
- Earth's albedo: fraction of radiation coming from the Sun that is reflected by the planet's surface, and it operates in the high-frequency band. It is related to the Absorptivity coefficient. Albedo is not constant and depends on various factors, including the seasons, regions traversed (illuminated side or shadow side), and altitude. Albedo is connected to the view factor, which considers the orientation of the surface;^[37]
- IR: this emission is related to the normal of the albedo flat plate in the outer planetary region. When the planet is in shadow, the emitted power is exclusively due to IR radiation;^[37]
- Shadow effects: they play an important role in altering the thermal conditions of the system. Acknowledge of the duration and evolution of the shadow effects helps determining which radiation effects have to be taken into account;^[37]

To manage the heat fluxes, TCS uses the yaw steering law to optimally orient the spacecraft. This orientation strategically positions the +X radiators facing deep space, allowing RAFTS (Rubidium Atomic Frequency Standards) and the power system to receive controlled sunlight exposure and maintain stable internal temperatures. Thus, it reduces the risk of overheating and ensuring minimal thermal variations that could impair sensitive onboard components. Indeed, the onboard systems, including the navigation signal generators and atomic clocks, generate considerable heat. Additionally, in the GIOVE-A mission case, it is useful to strategically position components on thermal interface materials (like gaskets and doublers) directly on the Y radiators, and install heat pipes under the high dissipative power amplifiers and the atomic clocks, promoting effective heat dissipation, homogeneous heat distribution on the radiators and, temperature stability and accuracy^[43].

About the internal heat flux, each component has an efficiency factor; the power used in the system is calculated by multiplying the obtained power by this efficiency factor. Identifying the worst-case scenario is essential, taking into account both the maximum and minimum incoming fluxes. All onboard dissipated power must be radiated into space, with the exception of specific cases like radiofrequency transmitted power.

1.2.2 Considerations on GIOVE-A Thermal Environment

During GIOVE-A's total mission span, the solar irradiance levels registered at 1 AU are around 1360 W/m^2 , which indicates a period of stable solar output with minimal sunspot numbers and radio fluxes. In operational phases, when the spacecraft is at MEO it was exposed to 1407.7 W/m^2 (closest to Sun) and 1315.7 W/m^2 (farthest from Sun), at perihelion and aphelion respectively. Almost 67% of solar radiation is absorbed by the Earth and re-emitted as IR heat flux. Earth's emissivity, usually between 0.6 to 1, is lower in deserts and semi-arid regions (below 0.85), due to atmospheric trapping of emitted radiation. This produces a mean surface temperature of 15°C . The remaining solar radiation is reflected as albedo flux, absent during eclipse, varying between 23.7 W/m^2 and 25.4 W/m^2 . Satellite measurements from NASA's CERES show global albedo averages around 30% which validates the observation^[44]. In case of the orbital raise, GIOVE-A experienced heat fluxes similar to the IOT phase as the spacecraft was only orbiting 113 km higher. There were minor thermal fluctuations due to Earth's orbital eccentricity that didn't warrant dedicated shielding or radiators for the entire satellite. Utilizing black coating for high emissivity to dissipate excess heat during regular solar exposure was useful, thus preventing overheating for the onboard setup. During eclipses, heaters maintained the temperatures of sensitive components. Additionally, from 2006 to 2008, several geomagnetic storms and solar flares occurred which impacted Giove-A and it was potentially resolved through a combination of MLI and path corrections^[45].

2 Sizing

2.1 Hot and Cold Cases Selection

To properly design the Thermal Control System, it is necessary to identify the most extreme thermal conditions, namely the coldest and hottest scenarios. To achieve this, the initial step involves estimating the internal heat generated by all active subsystems onboard, specific to each operational mode. As a first approximation, the internal heat generation can be assumed to be equal to the entire power budget of the satellite for a given mode. The following table details the internal power generated by each subsystem for each mode. All data presented below has been retrieved from the datasheets of the actual components used in GIOVE-A or, if not applicable, from datasheets of similar missions.

	Orbit Control Mode	Normal Mode	Safe Hold Mode	Stand-by Mode
Propulsion	87.8	58	58	58
TTMTC	51.5	51.5	51.5	51.5
AOCS	106.5	106.5	13	106.5
TCS	79	79	79	79
EPS	129	129	129	129
OBDH	5	5	5	5
P/L	36.7	156.7	-	-
total	495.5	585.7	335.5	429

Table 22 : Internal power generated [W]

As shown in the table, the highest internal heat generation occurs during the Normal Operations Mode. In this mode, the satellite experiences maximum power generation because all payload equipment is active. Consequently, the most extreme hot case is when the satellite is fully exposed to sunlight, maximizing heating from external sources, while operating in its Normal mode. Conversely, the lowest internal heat generation occurs during the Safe Hold Mode. During this mode, only the essential functions for satellite survival are active, resulting in minimal internal power generation. Therefore, the most extreme cold case occurs when the satellite is in eclipse and operating in Safe Hold mode.

2.2 Results

Following the definition of the preliminary architecture for the TCS and the selection of the most extreme hot and cold operational conditions, we proceeded with the initial sizing of the subsystem.

Input data		Results	
$\alpha_{coating}$	0.20	A_{ex}	2.98 m^2
$\epsilon_{coating}$	0.15	A_{rad}^{min}	1.52 m^2
ϵ_{Earth}	0.95	Q_{Sun}	813.79 W
ϵ_{rad}	0.88	Q_{albedo}	52.68 W
Q_{int}^{hot}	560 W	Q_{IR}	30.59 W
Q_{int}^{cold}	350 W	$Q_{heaters}$	285.44 W
T_{Earth}	15 °C	$T_{s/c}^{hot}$	73.23 °C
T_{DS}	-270.15 °C	$T_{s/c}^{cold}$	-25.53 °C
T_{max}	10 °C		
T_{min}	-5 °C		

Table 23 : Sizing numerical results

Our thermal analysis employed a mononodal model, which treats the spacecraft as a point with a fixed radiative area and constant optical properties. Specifically, we calculated the surface area of an equivalent sphere, $A_{eq} = 11.9 \text{ m}^2$, having the same volume as the actual GIOVE-A satellite. Different portions of this equivalent area were considered for the computation of various types of heat fluxes. In particular, for the computation of the Solar flux only the exposed area, $A_{ex} = A_{eq}/4$, has been used. The internally generated heat power for both the hot and cold conditions were calculated with the following rationale:

- For the worst hot case, which corresponds to the Normal Mode outside the eclipse period, the most significant sources of internal heat are given by the Payload, AOCS and power subsystems. We estimated the dissipated power, which is converted into heat, $Q_{int}^{hot} = 560 \text{ W}$, by retrieving the power consumption

of each subsystem as shown in the previous section and assuming that all active components in each mode contribute to the internal heat generation.

- For the worst cold case, which corresponds to the Safe Mode within the eclipse season, the most significant sources of internal heat are the thermal and power subsystems. We estimated the internally generated heat power for this condition using the same procedure as in the hot case, $Q_{int}^{cold} = 350 \text{ W}$.

The heaters installed on the thrusters were activated during orbital maneuvers. Despite being externally mounted, they contribute to the internal heat generation through conductive heat flux directed towards the satellite's main body.

For the external heat fluxes, we considered the presence of solar, albedo, and Earth's infrared heat flux for the hot case, while only the Earth's infrared heat flux was taken into account for the cold case. Each heat flux was computed and the heat balance equation was retrieved for both the worst hot case:

$$Q_{Sun} + Q_{albedo} + Q_{IR} + Q_{int}^{hot} - Q_{emitted} = 0 \quad (1)$$

and for the worst cold case:

$$Q_{IR} + Q_{int}^{cold} - Q_{emitted} = 0 \quad (2)$$

Subsequently, starting from these two equations, the satellite's temperatures in both the hot and cold cases were computed, assuming passive radiative cooling with deep space.

$$T_{sc}^{hot} = \sqrt[4]{\frac{Q_{int}^{hot} + Q_{Sun} + Q_{albedo} + Q_{IR}}{\sigma \epsilon_{coating} A_{eq}}} + T_{DS}^4 \quad (3)$$

$$T_{sc}^{cold} = \sqrt[4]{\frac{Q_{int}^{cold} + Q_{IR}}{\sigma \epsilon_{coating} A_{eq}}} + T_{DS}^4 \quad (4)$$

where σ is the Boltzmann constant and $\epsilon_{coating}$ is the coating emissivity assumed to be 0.15.

The temperature in the worst cold case exceeds the operational temperature range of [-5°C, 10°C], retrieved from the specifications of the most sensible components on board which are the RAES clocks, making the sizing of heaters in the thermal control subsystem design necessary to maintain the spacecraft temperature within the required range. Therefore the heat power required to the heaters has been computed as:

$$Q_{heaters} = \sigma \epsilon_{coating} A_{eq} T_{sc}^4 - Q_{IR} - Q_{int}^{cold} \quad (5)$$

The temperature in the worst hot case also exceeds the temperature range, for this reason radiators were sized, in order to cool down the spacecraft when needed, starting from the heat balance, considering the radiators emission contribute:

$$Q_{Sun} + Q_{albedo} + Q_{IR} + Q_{int}^{hot} - Q_{emitted} = \sigma \epsilon_{sc} A_{ex} T_{sc_{hot}}^4 + \sigma \epsilon_{rad} A_{rad} T_{DS}^4 \quad (6)$$

Considering then $T_{sc} = T_{max}$ the minimum radiators surface can be computed as:

$$A_{rad}^{min} = \frac{Q_{int}^{hot} + Q_{Sun} + Q_{albedo} + Q_{IR}}{\sigma \epsilon_{rad} (T_{sc_{hot}}^4 - T_{DS}^4)} - \frac{\epsilon_{coating}}{\epsilon_{rad}} A_{ex} \quad (7)$$

2.3 Adopted Control Strategy

GIOVE-A satellite is equipped with both active and passive controllers for its TCS subsystem.

We compared the temperatures predicted by our sizing model with the minimum and maximum allowed temperatures for all onboard components. The values are visible in the Table 3 (all the data have been retrieved from the proper datasheets).

This comparative analysis revealed that simple passive radiative cooling with deep space is insufficient to maintain the GIOVE-A satellite within the allowed temperature range, necessitating a more sophisticated thermal design and active thermal control.

Component	Operating temperature range
HGA (S-patch antenna) ^[46]	-20 °C to +50 °C
On-board Computer ^[47]	-20 °C to +50 °C
Tanks ^[48]	-20 °C to +50 °C
Power system ^[49]	-20 °C to +50 °C
Reaction wheels ^[50]	-20 °C to +50 °C
Sun sensors ^[30]	-40 °C to +80 °C
Magnetorquers MTR-30 ^[33]	-30 °C to +50 °C
Magnetometers ^[51]	-20 °C to +50 °C
Merlin and CEDEX ^[52]	-20 °C to +50 °C
Uplink receiver ^[53] and Downlink transmitter ^[54]	-20 °C to +50 °C
RAFS ^[55]	-5 °C to +10 °C

Table 24 : Real temperature ranges of GIOVE-A components

Consequently, a preliminary design of the radiator was carried out, estimating the minimum surface area (Table 1) needed to stay just below the maximum permissible temperature. Similarly, for the heaters, the minimum thermal power required to stay just above the minimum permissible temperature was estimated. The estimated power needed for the heaters is considerably higher than the actual power budget allocated to the active thermal control of the GIOVE-A satellite (see Table 4). This discrepancy arises from the assumptions made to perform the sizing, namely the mononodal model, and consideration of margins to take into account the worst case scenarios.

2.3.1 Active Thermal Control

The active thermal control provided by the TCS is performed through the utilization of **heaters** which are connected to the payload, power subsystem as well as the tanks and feeding lines of the propulsion subsystem (Figure 1). Those that are placed along the propulsion feeding lines are used to optimize the conditions for the utilization of liquid butane by regulating its temperature. However, during the actual mission, the heaters on the feeding lines remained inactive as thermal sensor data indicated that the tanks temperatures consistently remained around 30°C, avoiding the necessity for their activation^[56].

2.3.2 Passive Thermal Control

Unlike active systems that rely on power-consuming mechanisms, passive thermal control utilizes the principles of heat transfer and radiation to regulate temperatures passively. By strategic design considerations, GIOVE-A passive systems offer a reliable solution for managing thermal loads on the satellites.

Thermal blanket: Merlin and CEDEX instruments are mounted externally on the spacecraft, therefore they will be covered in a thermal blanket which provides some protection, ensuring the durability of the instruments against environmental factors^[52].

Thermal grease^[57]: it is used between radiators and platforms, but also between platforms and payload radiation to minimize thermal resistance, allowing heat to flow more effectively from the source to the radiating surfaces.

Radiators: the spacecraft's framework incorporates an aluminum honeycomb structure that functions both as a structural component and a radiator^[58]. Thermal management is primarily passive, utilizing the ± Y and +X panels as radiating surfaces for the payload. More precisely:

- the +X surface acts as a radiator for the RAES and power system
- the payload, situated on both -Y and +Y surfaces, uses these Y panels specifically for heat dissipation
- for more efficient heat release, the RF payload is directly attached to the Y radiator surface^[57].

Doublers: they are additional components to enhance the satellite's thermal capabilities. These passive aluminum plates expand the heat exchange area and distribute the equipment's dissipated heat across the radiator surface. Although functioning like a heat pipe, they are less efficient. In GIOVE-A, doublers link the RF

payload to the Y surfaces^[57] and also NSGU, FGUU and CMCU are mounted on them.

Since in space the optimum radiation efficiency is achieved by aiming the radiator at deep space, incorporating yaw steering modes for solar panel orientation minimizes direct Sun exposure on certain radiator surfaces. It helps maintaining optimal thermal conditions for the spacecraft and so, nominally, no Sun is illuminating +X radiators and also Y surfaces.^[57]. In fact, the +X panel is always deep space pointing and, being the solar panels perpendicular to the Y panels and constantly Sun-facing, the ± Y panels point away from the Sun and towards deep space as well.

Furthermore, in the current analysis, the assumption to coat the main body of GIOVE-A in black paint has been made. This decision is based on a combination of factors. Firstly, during the reverse sizing process of the TCS, it was determined that the system's components could reach a minimum temperature of -29 °C. Nevertheless, upon reviewing the actual datasheets of the components, which show a minimum sustainable temperature of for the most sensible element (Table 2), it was considered important to implement strategies to increase heat absorption.

2.4 Mass, Power and Data Budget

Heaters, as outlined in section 2.3.1., are connected to the payload bay, to the power subsystem and to the tanks. On board of GIOVE-A, 7 heaters are considered to be present, where only 5 are active (3 for the payload bay and 2 for the power subsystem to ensure the redundancy) being the two present near the tanks inactive as explained previously. Each of them consumes 8 W. Focusing on the radiators, the +Y and -Y faces are primary radiators while the +X face is a secondary radiator^[60]. Therefore the total area accounting for radiators would be of 8.25m² with a total weight of 1.65 kg^[61].

Additionaly, the Thermal Control System (TCS) subsystem is linked with other systems via temperature sensors to ensure each component maintains temperatures within acceptable thresholds. Specifically, GIOVE-A utilizes K-type thermocouples for this purpose and, as outlined in the datasheet^[59], each thruster is outfitted with three thermocouples for redundancy.

Due to the unspecified quantity of thermocouples for all the other components, a comprehensive and critical analysis was carried out to understand the components interfaced with the TCS subsystem. All the interconnections bewteen the subsystems are visible in Figure 2. An estimate of 90 thermocouples has been derived, considering that each component has a minimum of two thermal sensors to ensure redundancy in case of sensor failure.

Taking into account all the previous information, the mass and power budget of the whole system can be computed as follows:

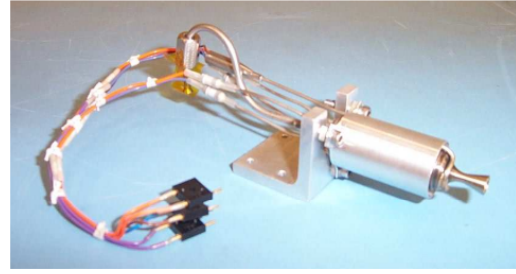


Figure 15 : GIOVE-A Resistojet with thermocouples^[59]

Components	N°	Mass Budget [Kg]	Power budget [W]
Heaters ^[62]	7	0.7	56
Radiators ^[61]	-	1.65	-
Thermocouples ^[63]	90	0.9	-
TDC ^[64]	90	0.00051	42.354
Total		3.25	98.354
Total with 20 % margin		3.9	118.0248

Table 25 : Mass and Power budgets

In mass budget computation the doublers and MLI were not included being lightweight. Additionally the power budget computed is the one accounting for the worst case scenario which is linked to the cold case. Thus, the comprehensive analysis results in a total power budget of 118 W designated for the Thermal Control System. Lastly, for data estimation purposes, GIOVE-A is equipped with Thermocouple-to-Digital Converter^[64] which can provide 14 bits of data for each sensor, therefore the total data budget is of 1260 bit.

ELECTRIC POWER SUBSYSTEM

1 EPS Subsystem

The electrical power subsystem (EPS) of a satellite is responsible for generating, storing and distributing the electricity needed to power all subsystems of the satellite. This includes the supply of energy for propulsion, sensors, telecommunications, navigation systems, and other payloads. Given the critical nature of these functions, the EPS must be designed to ensure a reliable energy supply, resistant to the extreme environmental conditions of space and able to adapt to the changing needs of the mission.

This paragraph will examine in depth the design, components and crucial considerations that guide the development of the power supply system of the satellite GIOVE-A.

1.1 EPS Design and Architecture

The EPS employs the 'GMP-D' design developed for SSTL's Gemini geostationary platform. It features a dual-voltage (27 V & 50 V) bus and boasts a modular structure, enabling scalability from approximately 400 W to 2 kW. During daylight operation, the 50 V is regulated from the solar arrays, while during eclipses, it is regulated from redundant regulators on the 60 Ah lithium-ion battery. The solar array drive mechanism enables Sun tracking by the wings while keeping the antenna fixed on its Earth target. The Power Control and Distribution System operates autonomously and exhibits fault tolerance.

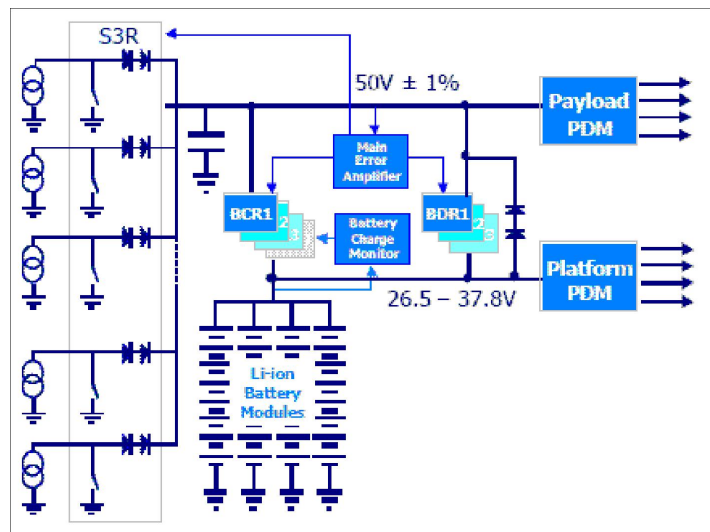


Figure 16 : Giove-A EPS block diagram^[7]

For Earth-orbiting mission the usual configuration is photovoltaic cells: they convert incident solar radiations directly into electric energy^[65]. So, as expected, GIOVE-A's solar arrays are equipped with RWE Hi-ETA2 Silicon solar cells, provided by Dutch Space BV, configured in 144 cells per string and 4 strings per panel. Each string constitutes an array section of maximum section current 1.1A. There are 4 panels, two per wing, equating to a total of 16 sections. The choice of Silicon over other materials like gallium-arsenide (which are better from a mass-area point of view) has to be imputed to economic budget reasons. Moreover, to get an optimal Sun incidence, solar arrays are panel mounted. This leads to the necessity of stricter requirements of pointing and tracking, accomplished by the presence of Sun sensors. In *Table 1* the expected and real current value are reported.

Solar Array section	Expected current on 28/12/2005 (mA)	Expected current on 27/02/2006 (mA)	Expected change (%)	Measured current on 28/12/2005 (mA)	Measured current on 27/02/2006 (mA)	Measured change (%)
2	1047	1017	-2.87	1010	983	-2.67
4	1044	1015	-2.78	1018	990	-2.75
6	1042	1013	-2.78	1007	984	-2.28
8	1058	1029	-2.74	1013	990	-2.27

Table 26 : Expected and measured current values^[66]

Control over the connection between the solar arrays and the payload is managed through a Sequential Switching Shunt Regulator (S3R), shunting the current away from the subsystem when loads or batteries do not need energy. The S3R comprises 16 shunt sections, with each section linked to a specific solar array section via the SADM (Solar Array Drive Mechanism). Shunt regulators guarantee high efficiency.

During eclipse operation, the battery supplies power to the payload through redundant Battery Discharge Regulators (BDR). Each BDR can handle up to 350W of power, and the failure of one regulator does not impact the essential battery discharge capability (high redundancy). GSTB-V2/A requires three BDRs in total. The unit accepts input voltages ranging from 26.5V to 37.8V, aligning with the nominal battery voltage range, and ensures a regulated 50V output with a tolerance of $\pm 1\%$. Over-voltage protection is integrated into the module design, aiming to promptly address any failed BDR unit or over-voltage situations within the power system. In *Figure 2*, a representation of operation of BDR: it takes over the regulation of the main bus as soon as the *S/C* reaches the eclipse; both the BDR output current and the load of the main bus are constant during eclipse, until the spacecraft has cooled down to the point when nominal operation heaters are automatically switched on to maintain the required operating temperature on the spacecraft.

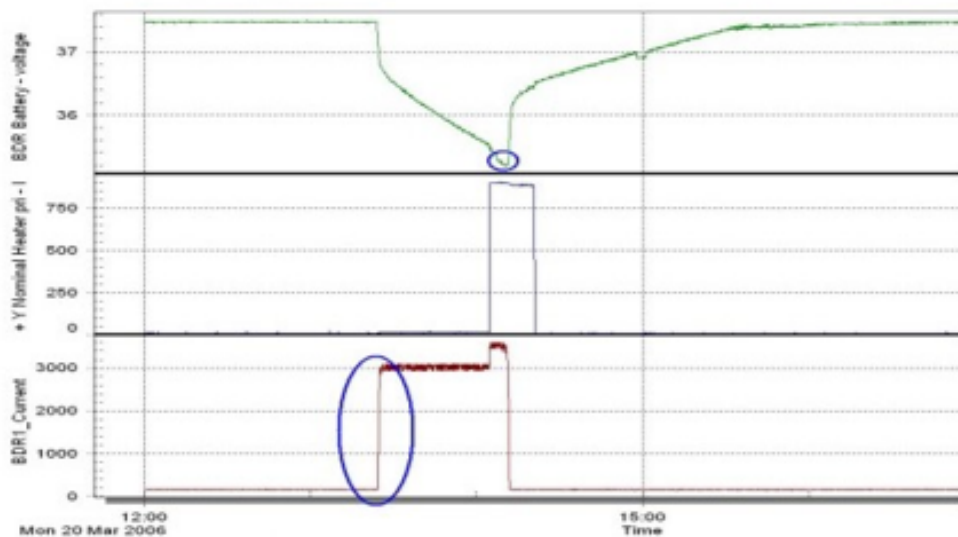


Figure 17 : BCR Operation and Battery Charging Sequence^[66]

During sunlight, the battery undergoes charging facilitated by the Battery Charge Regulators (BCR). Four BCRs are utilized for GSTB-V2/A, each connected to the payload bus. Detection of charge is achieved through a redundant, majority-voted analogue control loop that monitors battery voltage. The Battery Charge Monitor (BCM) circuitry, which controls battery charging, is situated alongside the BCR in a unified unit.

Each BCR, rated at 150W, maintains an efficiency of approximately 90% at full load and operates at a frequency of 100kHz.

Three primary protection features are integrated into the BCR circuit: input over-current protection via a Resettable Timed Current Limiter (RTCL), output over-current protection, and battery over-voltage protection. The RTCL provides continuous current limit protection in case of a short-circuit within the BCR electronics, recycling after a preset period to mitigate faults. Additionally, output over-current protection ensures that the BCR's output current remains within its rating, while battery over-voltage protection safeguards against potential voltage surges on the Battery Bus, employing a similar principle to BDR over-voltage protection.

The Main Error Amplifier (MEA) supervises the payload bus voltage, providing error voltage to regulate the main bus. It is fully redundant. The Power Distribution Module (PDM) manages power distribution via Timed Current Limiters (TCL) and fuses, with separate modules for payload and platform, each employing appropriate voltage switches. The battery voltage is aligned with the platform systems' input range, establishing a dedicated 'battery bus.'

To ensure power supply during eclipse periods, LEOP, and in case of sun pointing loss, a lithium-ion (Li-ion) battery is employed for energy storage. Li-ion technology was chosen due to its ability to meet strict mass and volume constraints. For GSTB-V2/A, a battery capacity of 60Ah or 1950Whrs is required. This is achieved by connecting four parallel-connected 9s10p (9 series cells per string and 10 strings in parallel) modules, each delivering 15Ah at a maximum terminal voltage of 37.8V^[67]. Lithium-batteries are qualified for planetary missions, thanks to their great energy density and wide operating temperature range.

2 EPS Reverse Sizing

The reverse sizing has been carried out to design the electric power subsystem, consisting of solar arrays as primary electric source and of a Li-Ion battery as secondary electric source.

2.1 Power Budgets

Subsystem	LEOP		IOT/E-IOT/RO		EOL	Eclipse
	Operational	Communication	Normal	Communication	Orbit Control	
PS	58	0	58	0	87.8	0
TMTC	1.5	51.5	51.5	51.5	51.5	1.5
AOCS	106.5	106.5	106.5		13	13
TCS	79	79	79	79	79	110
EPS	129	129	129	129	129	129
OBDH	5	5	5	5	5	5
PL	0	6.7	156.7	156.7	36.7	36.7
Total	379	377.7	585.7	527.7	402	295.2
Total Margined (+20%)	451.2	453.24	702.84	633.2	482.4	354.2

Table 27 : Power budget per phase per mode

The values in the table are derived from the datasheets of GIOVE-A's components and a critical analysis of events in various phases and modes. Moreover, for GIOVE-A, the launch phase is not considered as the satellite was directly placed into orbit by the Soyuz-Fregat launcher.

Since GIOVE-A is constantly on a MEO orbit, power consumption of the PS remains stable, with no major maneuvers required except for one at the EOL to move the satellite to a higher orbit, which justifies a higher power consumption for this subsystem at this phase. More precisely, the propulsion system consists of 10 thrusters, each with a power of 15W, but only 3 thrusters are used at a time^[17]. Additionally, 8 valves operate simultaneously, each consuming 1.6W. The power consumed by the thrusters is also included in the AOCS, since between the 5 thrusters on GIOVE-A some of them are used for attitude control as well.

The AOCS's power consumption is constant across all modes, as the sensors and actuators are always active. In fact, the function of the AOCS is to de-tumble the satellite immediately after launch, to provide 3-axis stabilisation for the spacecraft within the required pointing tolerances, during nominal operations and orbit correction manoeuvres, and to control the spacecraft into a safe mode if non-nominal situations arise^[68]. The primary contribution is given by 4 reaction wheels configured in a pyramid, with 3 operating simultaneously, each consuming an average of 16.3W^[50]. Additional contributions come from 3 magnetorquers consuming 3W^[33] when all are active, and 16 sun sensors consuming 1.6W collectively (including redundant ones). The two Earth horizon sensors' power consumption is about 8W^[29] while inertial sensors are also present for redundancy^[68] but they are never used in the actual mission, therefore they are not considered in the computation.

Regarding TMTC, its peak power consumption is reached in Communication and Normal modes since in these ones a higher amount of data is required to be transmitted to the ground^[54]. The TMTC power budget remains high and constant during the overall mission since GIOVE-A is an in-orbit testing element requiring a constant communication with the Ground segment. Furthermore, in Operational mode, only the uplink receiver^[53] is assumed to be active because the payload commissioning is occurring in the LEOP.

The OBDH's power consumption is equal to 5W^[47]. More precisely, GIOVE-A employs two OBC386 modules in a cold redundant configuration.

The payload on GIOVE-A is divided into navigation, experimental, and environmental categories. The experimental payload, including CEDEX and Merlin, and the navigation payload are always active to meet mission goals and to ensure continuous data generation and transmission via the S-band RF communication system. CEDEX consumes 4.2W^[69], Merlin 2.5W^[52], NAVANT 120W^[70] and the RAFS 30W^[55]. An important aspect regarding the payload is that in the LEOP phase only the radiation monitoring sensors (Merlin and CEDEX) are activated. While regarding the Orbit Control mode, the NAVANT is turned off.

The EPS power budget has been retrieved from the computations made in Section 2.4.

Lastly, the Thermal Control System (TCS) includes 7 heaters (2 for feeding lines, 3 for the payload bay, 2 for the power system), each consuming 15W and 5% was assumed to take into account the thermal sensors. However, only 5 heaters are typically active as the feeding line heaters are not needed due to stable tank temperatures. Again, being GIOVE-A constantly in a MEO orbit, it experiences minimal thermal changes except during eclipse periods. Indeed during these periods, power consumption of other subsystems decreases: TMTTC reaches its minimum since the spacecraft communication are limited to subsystem health and telemetry, the AOCS reaction wheels are on standby consuming only 3.3W^[50], and also the payload activity is assumed to be reduced since only the environmental payload continues to operate in order to characterize the MEO orbit. On the other hand, the TCS reaches its peaks, since it operates at maximum to maintain feasible temperatures without solar heating.

2.2 Solar Array Sizing

2.2.1 Results

For the SA sizing a sunlight regulated bus voltage power system was chosen together with a Direct Energy Transfer regulator. This power control is more suitable for medium-long term missions, however it was chosen for the sizing process since it is simpler, more efficient and lighter than the PPT. In addition, DET is the actual control method adopted in the real GIOVE-A's EPS design^[67].

Input data		Results	
ϵ_{BOL} ^[71]	0.28	t_{Al}	$3 \times 10^{-2} m$
ρ_{Al} ^[72]	112 kg/m ³	t_{GaAs}	$400 \times 10^{-6} m$
ρ_{Si} ^[73]	2330 kg/m ³	T_d	13 h
θ	0 rad	T_e	1 h
A_{cell} ^[74]	0.0046 m ²	T_{Life}	19723.5 h
dpy ^[37]	0.0275	T_{period}	14 h
I_D ^[37]	0.5	V_{syst} ^[67]	50 V
I_0 ^[37]	1366.1 W/m ²	V_{cell}	2.6 V
P_d	600 W	X_d ^[37]	0.80
P_e	354.3 W	X_e ^[37]	0.60
		N_{real}	1120
		P_{BOL}	191.25 W
		P_{in}	382.51 W
		P_{EOL}	179.62 W
		P_{SA}	932.94 W
		N_{series}	20

Table 28 : SA sizing input data and results

In order to perform the solar array sizing it is necessary to identify the worst case scenario, hence the most demanding power request for both daylight and eclipse times. From the power budget (Table 2) we can deduce that the most demanding power requirement in daylight time comes from the Normal mode.

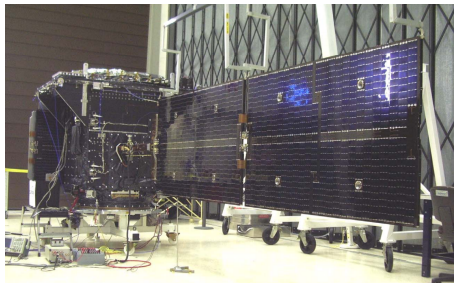


Figure 18 : GIOVE-A solar array^[67]

For the computation of the total requested power from the SA the daylight and eclipse times were derived. Given GIOVE-B eclipse time^[75], since GIOVE-A and GIOVE-B have the same orbit, GIOVE-A eclipse time coincides with GIOVE-B's. Knowing then the orbital period of the spacecraft, the daylight time was computed as $T_d = T_{period} - T_e$. The nominal mission duration was of 27 months, therefore any extension of the mission lifetime was not taken into account during the sizing.

For the Sun irradiance we considered its average value with respect to Earth being GIOVE-A a planetary mission. Using the SA efficiency at BOL and the Sun irradiance, the specific power output can be computed. The SA specific power depends on θ , the inclination angle between the array surface normal and the Sun direction, which is assumed to be zero in the sizing, since the solar arrays are always Sun-facing as this is one of the main pointing requirements of the mission. Considering that GIOVE-A solar arrays are made of three-junction cells, the inherent degradation is assumed to be equal to 0.5, which is a typical performance value for multi-junction cells. Knowing the specific power at BOL and the cell degradation, which is assumed to be 0.0275 for Silicon cells^[37], the lifetime degradation was computed and subsequently the specific SA power produced at EOL was derived. The SA area was obtained considering the ratio between the requested SA power and the specific power at EOL. This value of the area is the minimum required to get the demanded power. However, it is smaller with respect to the actual SA area used on GIOVE-A, in fact the real power output per wing at summer solstice, at EOL, is 667 W^[7] for a total power output of 1334 W, therefore, the SA used in the actual mission have been oversized and this explains the discrepancy with our results from the sizing. Having computed the SA area and

assuming a multi-layer structure made of Silicon and Aluminum honeycomb, we can compute the SA mass.

The sizing was then refined computing the number of cells needed to cover the desired surface considering an average area of a single cell equal to $0.0046m^2$. Assuming a system voltage of 50 V, since the payload operates at this voltage (regulated bus), and assuming a cell voltage of 2.6 V, it was found that we need about 20 cells in series to get the desired voltage. We can then compute the actual voltage and actual number of cells needed to provide the desired voltage.

The rationale behind the selection of the most optimal primary power source is based on an assessment of the spacecraft's power demands, which in the case of GIOVE-A satellite ranges from 500W to 2kW^[67], and the mission's lifespan (2 years for the nominal mission). Given these power demands and lifespan, the solar array solution effectively meets both requirements, hence it has been chosen as the primary power source for this mission.

2.2.2 Positioning and Pointing

For the GIOVE-A satellite, the solar arrays are symmetrically positioned along the Y faces of the main structure. The precise placement of the solar panels relative to the main body is not critical because the orientation of the solar arrays is independent from that of the main body, facilitated by the Solar Array Drive Mechanism (SADM)^[42] which is an electromechanical actuator, that enables the solar arrays to rotate around the Y-axis independently from the spacecraft. This feature is essential as it meets both the requirements for the main body to point towards Earth and the solar arrays to point towards the Sun. Consequently, the SADM guarantees the effective functioning of the solar arrays regardless of the spacecraft's orientation. Hence, the most critical requirement for the EPS is ensuring that the solar panels always face the Sun.

2.3 Battery Sizing

2.3.1 Results

For the battery sizing a single Li-Ion battery was chosen as it was the one employed in the real mission design. The sizing was performed at EOL, in order to grant correct battery operations throughout the whole mission duration.

Input Data		Results	
$\eta^{[37]}$	0.4	C	1.77×10^3 Wh
$\mu^{[37]}$	0.8	C_A	63.25 Ah
$C_{cell_{batt}}$	7.5 Ah	C_{string}	302.4 Ah
DoD	0.5	C_{real}	1.81×10^3 Wh
$E_m^{[37]}$	140 Wh/Kg	m_{batt}	12.65 Kg
$E_v^{[37]}$	250 Wh/dm ³	$N_{parallel}$	6
$N_{batteries}$	1	$N_{series_{batt}}$	14
P_R	354.2 W	$Volume_{batt}$	7.08 dm ³
T_R	1 h	$V_{batt_{real}}$	50.4 V
$V_{cell_{batt}}$	3.6 V		
$V_{sysbatt}^{[67]}$	28 V		

To size the battery we firstly have to identify the time window during which it must provide power and the requested power for the most critical mode. It was deduced that $T_R = T_e$ and $P_R = P_e$ since the battery is the secondary power source and shall provide the needed power to the s/c during eclipses, when the SA cannot be used.

Typical values of the specific energy, the energy density and the efficiency for Li-Ion batteries were considered^[37]. The nominal lifetime of GIOVE-A is 27 months and the spacecraft period is about 14 hours with 1 hour of eclipse per orbit, hence it is a relatively short mission with a high number of cycles, for this reason the DoD value was assumed to be 0.5.

The required battery capacity to fulfil the power demand was computed knowing the efficiency, the eclipse time, the power request and the DoD. Subsequently, knowing the battery capacity, the specific energy and the energy density we can compute the mass and the area of the battery.

To refine the sizing we assumed a cell voltage of 3.6V and a system voltage of 28V, since the platform operates at 28 V through an unregulated bus. From this values we can retrieve the number of cells to put in series to get the desired voltage and with this value, together with the voltage of a single cell, we can retrieve

the real voltage of the system. The capacity of a single string is then computed assuming typical values of the package efficiency of the single cell capacity^[37].

In the end we computed the actual number of strings to put in parallel and the actual battery system capacity. Li-ion technology was selected in order to meet the tight mass and volume constraints, in fact we can see that the battery volume and mass are reasonable and close to the real ones. As for the battery topology we have 4 parallel modules, each module consisting of 9 cells per string for 10 strings in parallel. This topology choice finds its rationale in redundancy and safety since it grants the correct functioning of the other cells in case of the failure of one of them.

2.3.2 Positioning

The four battery cells are located internally on the $Z+$ face of the satellite^[7]. This face remains non-Sun-pointing as the satellite's nominal attitude is nadir-pointing to improve communication and enable testing of the NAVANT antenna. Consequently, the batteries are shielded from direct solar heat flux and the thermal extremes of deep space. This configuration ensures that the batteries maintain an optimal thermal environment, preventing overheating and excessively low temperatures, and thereby ensuring proper operational performance.

2.4 Budgets



Figure 19 : PDM and MEA^[76]

The calculations for the mass, volume, and power budget of the GIOVE-A's EPS subsystem have taken into account the presence of the Li-ion battery, the solar arrays with their driving mechanisms, and all the power system components, including three BDRs, four BCRs connected to the payload bus, one MEA, and two PDMs (one for the payload and one for the platform)^[67].

The power budget of the EPS components can be assessed by considering the output power it delivers to the payload and platform, along with the power transfer efficiency of each component. These efficiencies typically exceeds 90%: each BDR has an efficiency of 94% and an output power of 350W, BCR is rated to 150W and has an efficiency of about 90% while the PDMs have an efficiency higher than 99%^[67]. The high efficiency values indicate that the majority of the power is directed towards the payload and platform. However, a small percentage is consumed by the EPS components for their operation.

Mass budget [Kg]								
Battery	SA	SADM	BDR	BCR	MEA	PDM	Total	Margined [20%]
15.8	19.58	6	3	4.2	2.45	1.9	52.93	63.52

Table 29 : EPS mass budget^{[76][77][42]}

Power budget [W]				
SADM	BDR	BCR	Total	Margined [20%]
6	63	60	129	154.8

Table 30 : EPS power budget^{[67][42]}

Volume budget [m^3]							
SA-stowed	BDR	BCR	MEA	PDM	Battery	Total	Margined [20%]
3.41	0.00226	0.00226	0.00169	0.00226	0.000769	3.42	4.092

Table 31 : PS volume budget^[76]

Lastly, EPS includes a majority voted analog control loop to monitor the battery. More specifically, the Battery Charge Monitor (BCM) and Main Error Amplifier (MEA) within this system are both majority voted and redundant, enhancing reliability^[67]. Being an analog circuit, ADC components are needed, such as the ADS1115^[64] which fits in the operability range of GIOVE-A. They can convert analog signals to digital, facilitating precise majority voting to determine the end of charge detection and maintain system accuracy. Therefore, considering that a majority voter is composed of 3 sensors (each with its own ADC of 16 bit) and assuming that 36 ADCs are present in a redundant configuration in all the four BMCS while 6 ADCs are connected to the single MEA, we obtained a data budget of $DATA_{EPS} = 806$ bit, assuming a 20% margin.

SPACE SEGMENT CONFIGURATION

1 CONF System

Configuration of space segment is meticulously designed to meet operational needs, technical requirements, and the constraints imposed by its launch vehicle.

1.1 Overall Vehicle Shape and Appendages Distribution

The satellite features a compact, box-shaped main body^[7]. This configuration is optimal to house the primary payload, such as navigation instruments, atomic clocks, and the subsystems necessary for its mission (*Figure 1*). Another crucial aspect is the appendages of GIOVE-A: they are disposed to maximize operational efficiency, through maintain a great balance in the structure. The most prominent appendages are the solar panels which are mounted on the side of the satellite body. They are stowed during launch and deployed once the satellite reaches orbit. Additionally, GIOVE-A is equipped with antennas for navigation (NAVANT) and telemetry, tracking, and command (TT&C) operations. After a meticulous study of the attitude of the spacecraft, the solar arrays and antenna are placed as in *Figure 2*, to accomplish the following requirements:

- Pointing: solar arrays must point in Sun direction, meanwhile the antenna is Nadir pointing;
- Clearness in FOV: the placement of the antennas is calculated to avoid interference and ensure clear signal transmission, meanwhile the deployment mechanism of solar panel is designed to avoid interference with other appendages and to maintain the satellite's balance and stability.

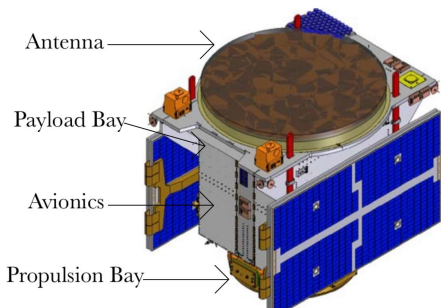


Figure 20 : General Giove-A configuration

1.2 Launcher Interface Location and Features

The interface between GIOVE-A and its launch vehicle, a Soyuz-Fregat rocket (*Figure 3*), is a vital component of the satellite's design^[7]. The launch vehicle interface is located at the base of the satellite, where it connects to the rocket's payload adapter. This interface must securely hold the satellite during the high-stress conditions of launch and facilitate a smooth separation once in orbit. Key features of the launcher interface include:

- Mechanical attachment points: designed to withstand the forces encountered during launch, such as vibrations and accelerations;
- Electrical connectors: used for pre-launch testing and for providing power and communication between the satellite and the launch vehicle's systems.

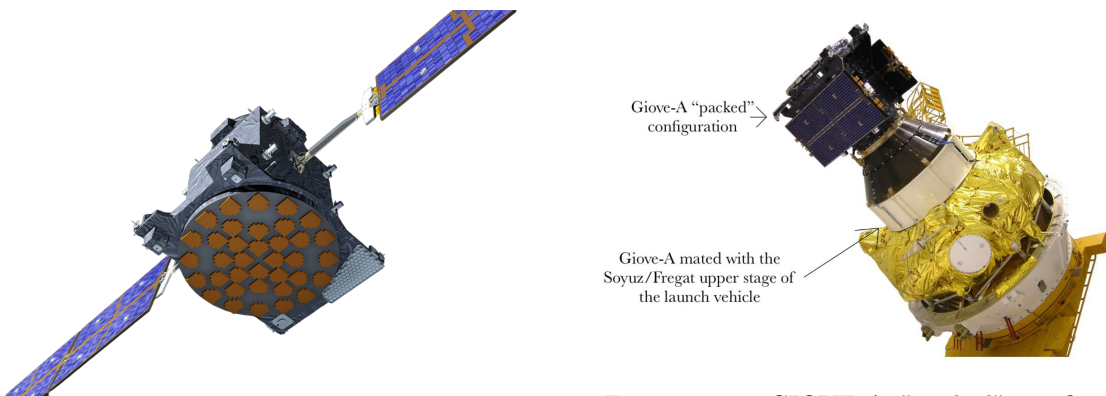


Figure 21 : Giove-A "unpacked" configuration

Figure 22 : GIOVE-A "packed" configuration and connection with Soyuz/Fregat launcher upper stage

1.3 Vehicle Configuration in the Launcher Fairing

During launch, GIOVE-A is housed within the payload fairing of the Soyuz-Fregat rocket ('packed' configuration - *Figure 3*). The fairing protects the satellite from aerodynamic forces, heating, and contamination during the

ascent through the Earth's atmosphere^[37]. As said before, solar panels are stowed to minimize occupied volume. Different factors have been considered for the general geometry in this first part of the mission. First, the available space within the fairing dictates the maximum dimensions of the satellite in its stowed compact form. Secondly, to ensure stability during launch, the centre of mass must be precisely controlled. This is achieved by placing heavier components towards the base and balancing the distribution of mass around the central axis of the spacecraft.

Furthermore, transportation requirements necessitate that GIOVE-A is robust enough to withstand the rigors of handling and integration with the launch vehicle. This includes ensuring that the satellite's structure can endure the mechanical stresses of transportation to the launch site and integration processes.

1.4 Distribution and Location of Elements

The design and arrangement of components on a satellite require careful considerations of various engineering and functional factors. Each element must be positioned optimally to ensure the operational efficiency, structural stability and durability of the satellite itself. This section explores the motivations, through a detailed analysis of the positioning criteria, underlying the strategic placement of the main components on the satellite.

1.4.1 External Components

In this section, the positions of the main external components of the satellite will be analyzed, as represented and described in detail in *Figure 4*. Components examined include Earth sensors, Sun sensors, thruster^[34], SSTL S-band receivers^[78], dual antennas^[78] and solar arrays^[79].

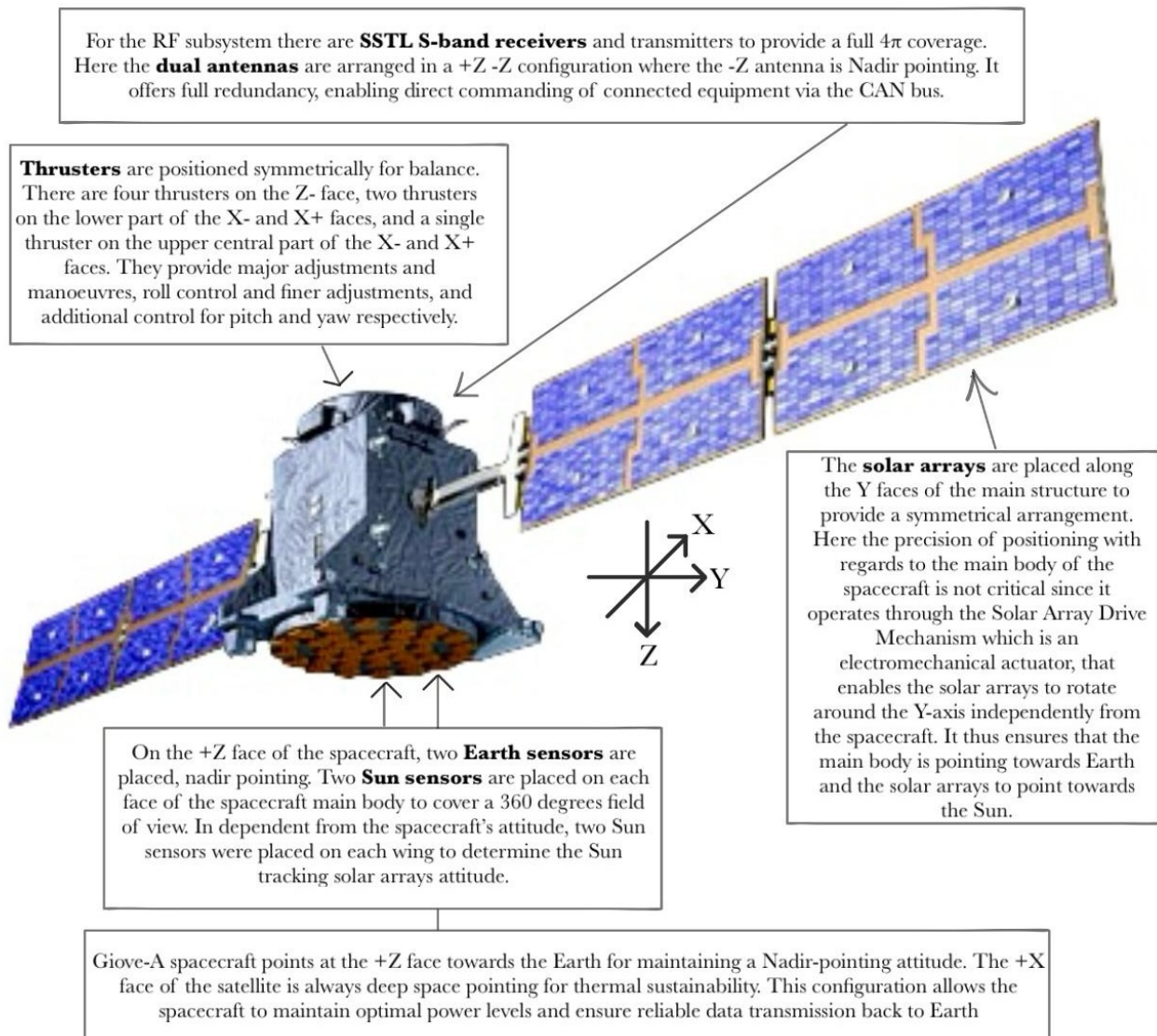


Figure 23 : External Elements Giove-A

1.4.2 Internal Components

This section explores in detail the internal components of the satellite, highlighting the functionality and arrangement of various critical elements for its operation. Among the components analyzed are propellant tanks, magnetorquers and reaction wheels, platform and payload units and battery cells^{[80][81][82]} and battery cells^[7]. The arrangement and integration of these components are crucial to ensure the reliability, energy efficiency and operational capabilities of the satellite during its mission.

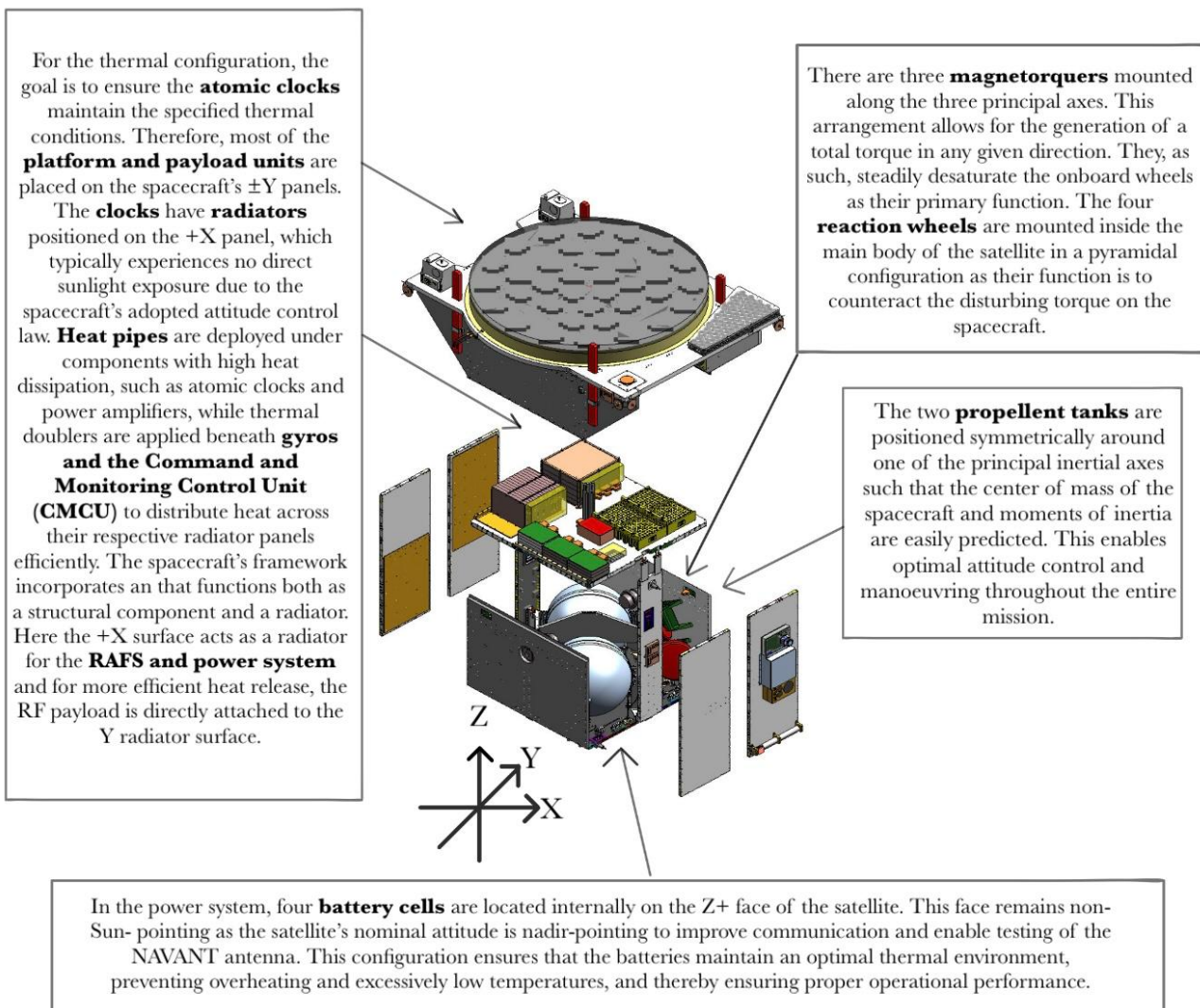


Figure 24 : Internal Elements Giove-A

ON BOARD DATA HANDLING SUBSYSTEM

1 OBDH Subsystem

The OBDH subsystem serves as the "brain" of the GIOVE-A platform and allows the satellite and its payloads to function with a high degree of autonomy^[83]. The OBDH subsystem is responsible for a range of essential tasks, including the execution of guidance and control algorithms, the collection and storage of scientific data from the payload, and the management of uplink commands and telemetry. Additionally, it must feature autonomous failure detection and management capabilities to maintain spacecraft operations during emergency situations when standard communication with ground control is not possible. Additional key functions of the GIOVE-A's OBDH include monitoring the spacecraft's functionality and health, scheduling and supporting payloads, attitude control, power system management, data logging and processing, system backup, and communication support^[83]. Indeed, the OBDH subsystem incorporates Telemetry and Telecommand Networks and On-Board Computers (OBCs).

In essence, the primary functionalities of the OBDH subsystem are divided into two main categories: platform control and housekeeping. Platform control involves managing and controlling the satellite's core systems to ensure it remains operational and stable. Housekeeping refers to the routine monitoring and management of the spacecraft's health and status.

1.1 Architecture and Rationale

The data-handling system architecture is divided into three sections: CAN bus, OBC386 and ASM (Attitude safety module).

For the GIOVE-A mission, SSTL chose to use all in-house products with a well-proven heritage and experience. This decision was likely driven by the need to adhere to a tight schedule and meet the allocated timeframe to secure the ITU frequencies, which represented one of the main drivers of the GIOVE-A mission.

1.1.1 CAN Bus

The CAN bus has been utilized by SSTL in several past missions, proving its reliability and efficiency. In the GIOVE-A mission, a redundant Controller Area Network (CAN) bus is employed in a distributed telemetry and telecommand network. All the other modules are connected to the CAN as visible in the Figure 4 where the bus is represented by the black line.

One of the key features of the CAN bus is its ability to enhance system safety. The redundancy of the CAN bus ensures reliability, and its lossless bus bandwidth arbitration^[84] further contributes to its robustness: when multiple nodes attempt to send messages simultaneously, the CAN bus uses a bitwise arbitration process (each message has its own identifier) to determine which message gets transmitted first. The highest priority message wins, and the lower priority nodes automatically retry their transmission once the bus is free. This process ensures that no information is lost and allows the CAN bus to operate at high efficiency, making optimal use of the available bandwidth^[84]. Additionally, the lack of collisions and the elimination of the need for re-transmissions reduce latency, which is crucial for the time-sensitive operations of space missions.

The choice of a high-capacity bus and the emphasis on transfer efficiency are driven by the high data rates required for uplink and downlink communications (9600 bits/second). The CAN bus not only ensures high reliability but is also cost-effective. It is particularly well-suited for small to medium-sized spacecraft, like GIOVE-A, due to its simple two-wire bus topology, which reduces wiring complexity and saves both space and costs by eliminating wiring harnesses.^[85]

Lastly, GIOVE-A CAN TTC nodes have the capability to autonomously switch between primary and secondary buses if a bus lockup condition is detected, further enhancing the system's reliability and fault tolerance.^[86]

1.1.2 OBC386

In the GIOVE-A configuration, two OBC386 modules operate in a cold redundant setup, ensuring reliability and fault tolerance. A key aspect of the subsystem architecture is the integration of both OBC386 with the primary and redundant CAN bus system which, in turn, connects both of the computers to the spacecraft's S-band receivers and transmitters^[86], facilitating communication and control.

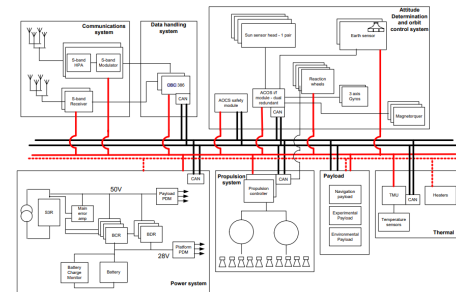


Figure 25 : Overall Giove-A CAN bus connections

Furthermore, the OBC368 module has full access to sensor data generated by the AOCS module, including inputs from sun sensors, gyroscopes, and Earth horizon sensors and it provides commands to the actuators (magnetorquer, wheel, propulsion)^[86]. This integrated approach ensures efficient data exchange and precise control over spacecraft functions, contributing to the overall success of the GIOVE-A mission.

Specifications: The OBC368 is equipped with an 80386EX CPU operating at 33 MHz. To enhance the computational capabilities of the CPU a 386SL coprocessor is used which allows to have faster and more efficient processing. The On-board computers also have a bootstrap ROM and a Ramdisk of 128 Mbytes in total. Lastly the OBC368 has 8/16/20/25 MHz clock which allows the computer to operate at different clock speeds^[87], this allows to have a more flexibility in processing power and energy consumption.

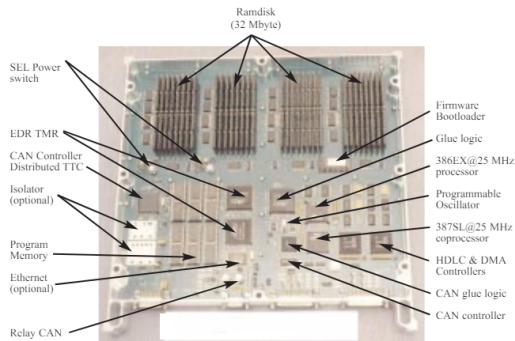


Figure 26 : Giove-A actual OBC368^[83]

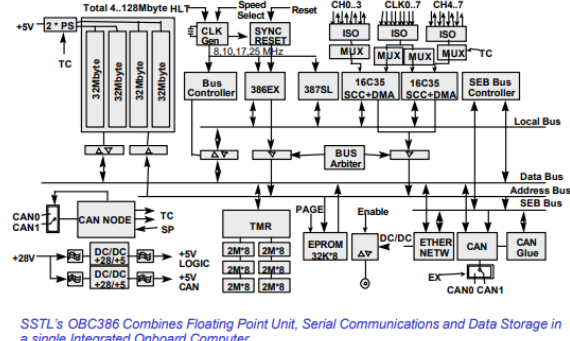


Figure 27 : GIOVE-A OBC368 schematics^[87]

Serial DMA (Direct Memory Access) links with the S-band RF systems: OBDH system is equipped with a dedicated link specifically designed to establish exclusive communication lines between the OBC368 and the S-band RF systems^[86]. This specialized link ensures reliable and uninterrupted data transmission. Furthermore, the DMA technology allows certain hardware subsystems to access the RAM independently of the central processing unit (CPU)^[86]. This strategic choice facilitates efficient data transfer between the OBC and the S-band RF systems without overburdening the CPU. By offloading data transfer tasks to the DMA, the OBC368 can handle large volumes of data more swiftly and efficiently. This optimization, therefore, is particularly beneficial for GIOVE-A, which encounters significant data processing demands.

BekTek SCOS (Spacecraft Operating System): It is a specialized software environment designed to manage and control the various functions of a spacecraft. Operating as a multi-tasking system, it can run multiple task concurrently, which is essential for managing the numerous and often simultaneous operations required in spacecraft control. Within this operating system, we find^[86]:

- **Memory Management:** it is responsible for the allocation, deallocation, and comprehensive management of the system's memory. Effective memory management ensures that each task receives adequate memory allocation to be executed without interference from other tasks. Moreover, it optimizes the utilization of available memory resources
- **Inter-Task Messaging:** the BekTek SCOS facilitates efficient communication between tasks, ensuring prompt response to events
- **Task Management:** it encompasses the creation, scheduling, and supervision of tasks or processes within the operating system. Task management ensures that each task is given the appropriate amount of CPU time, prioritizes critical tasks, and manages the overall execution flow to maintain system stability and performance

EDAC (Error Detection and correction) protected file system: It is used to identify and correct errors in both data storage and transmission processes^[86]. Within the file system context, EDAC protection safeguards data integrity by correcting any errors that arise. This capability holds particular significance in space missions, where the harsh environment, like radiation exposure that GIOVE-A encounters in its MEO orbit, poses risks of data corruption. 4 Mbytes is the amount of memory available with EDAC protection program RAM.

Low-level TTC Services: These systems are present to collect and transmit telemetry data, tracking the spacecraft's position and trajectory, and receiving commands from ground control^[86]. Unlike higher-level

services that involve complex data processing or decision-making, these systems primarily handle basic communication and data transmission tasks essential for maintaining connectivity and ensuring basic functionalities. So, their operations typically involve straightforward processes without extensive computational or analytical requirements.

1.1.3 ASM

The redundancy of the OBDH subsystem is meticulously ensured, not only through hardware redundancy with a redundant CAN BUS and two redundant OBC386 units but also through a strategic approach to system safety. This method incorporates a non-redundant Attitude Safety Module (ASM), which serves as the highest level of control for GIOVE-A. Post-launch, the ASM manages critical functions such as de-tumble and Sun-acquisition. Throughout the operational phase, it acts as a watchdog, monitoring the primary units and switching to secondary units in case of failure. Additionally, the ASM is equipped with simple attitude control algorithms leveraging Sun-sensors, gyros, and thrusters to maintain Sun-pointing orientation in the event of OBC386 failure^[86].

Moreover, all SSTL spacecraft feature 'back door connections' between spacecraft receivers and the power system. These connections enable direct control over unit activation or deactivation from ground stations, bypassing the CAN bus^[86]. This additional layer of control enhances subsystem efficiency and boosters safety measures.

1.2 OBDH Reverse Sizing

In the process of reverse sizing of the OBDH subsystem, an initial estimation is conducted to determine the dimensions of the subsystem's Memory (RAM and ROM) and the CPU (throughput and frequency). Given that this is an initial examination, statistical data, averaged across a broad spectrum of missions, will be employed to make a comparative estimation. In subsequent refinement stages, mission-specific values should be taken into account.

1.2.1 OBDH Functions and Elements

The first step to carry out the reverse sizing is to identify all the functions that the OBDH subsystem shall perform for each subsystem controlled by it. The main functions and elements are collected in the following table:

ADCS	EPS	PS
RW control	Voltage control	Engine control (2)
Thrusters control	Current control	Valves control (12)
Sun sensors (16)	Solar panels	Pressure sensor control (12)
Magnetotorquers (3)	Battery	Tanks (2)
Earth sensors (2)	Cable and harness	Heaters (10)
IMU (6)		
Kinetic integration		
Error determination		
Attitude determination		
Attitude control		
Ephemeris calculation		
Orbit propagation		

TMTTC	TCS
Transponder (2)	Heaters (7)

Table 32 : OBDH functions and elements

After having identified the OBDH functions, we define the real-time execution frequency for each element and then we estimate the throughput requirements for each function by-similarity knowing the wanted acquisition frequency^[37], through the following formula:

$$KIPS = \frac{KIPS_{typ} f_{acq}}{f_{typ}} \quad (1)$$

Subsequently, we can compute the total throughput needed by each subsystem expressed in thousands of instructions per second as well as the total data and code for all the subsystems expressed in words.

Knowing the throughput, code and data requirements, we can proceed with the sizing of the OBDH by evaluating the ROM and RAM both expressed in kilobytes. The used formulas are the following:

$$ROM [kB] = \frac{Code [words] 16 \frac{bit}{word}}{8 \frac{bit}{Byte} 1000 \frac{Byte}{kByte}} \quad (2)$$

$$RAM[kB] = \frac{(Code [words] + Data [words]) 16 \frac{bit}{words}}{8 \frac{bit}{byte} 1000 \frac{byte}{kByte}} \quad (3)$$

The following table displays the numerical results of the comparative estimation analysis for each subsystem for three different modes: the Communication mode, the Orbit Control mode (manoeuvre mode) and the Operational mode. The payload is excluded from the analysis under the assumption that it runs on its own dedicated CPU, simplifying the initial sizing process. Note that, to account for the high uncertainty linked to the statistical analysis, a 400% margin has been applied to all the numerical results.

	ACDS	EPS	PS	TCS	TMTC	OS	TOT	ROM [kB]	RAM [kB]	TP [KIPS]
Communication	1	1	0	1	1	1				
Throughput [KIPS]	704	1	0	3	30	173	911			911
Margined [KIPS]	3519	5	0	15	150	865	4554			4554
Code [words]	75900	2400	0	800	6000	36400	121500	243	243	
Margined [words]	379500	12000	0	4000	30000	182000	607500	1215	1215	
Data [words]	50500	1000	0	1500	19500	28300	100800			201.6
Margined [words]	252500	5000	0	7500	97500	141500	504000			1008
Orbit Control	1	1	1	1	0	1				
Throughput [KIPS]	704	1	89	3	0	173	969.8			970
Margined [KIPS]	3519	5	445	15	0	865	4849			4849
Code [words]	75900	2400	23600	800	0	36400	139100	278.8	278.8	
Margined [words]	379500	12000	118000	4000	0	182000	695500	1319	1319	
Data [words]	50500	1000	43500	1500	0	28300	124800			249.6
Margined [words]	252500	5000	217500	7500	0	141500	624000			1248
Operational	1	1	1	1	1	1				
Throughput [KIPS]	704	1	89	3	30	173	1000			1000
Margined [words]	3519	5	445	15	150	865	5000			5000
Code [words]	75900	2400	23600	800	6000	36400	145100	290.2	290.2	
Margined [words]	379500	12000	118000	4000	30000	182000	725500	1451	1451	
Data [words]	50500	1000	43500	1500	19500	28300	144300			288.6
Margined [words]	252500	5000	217500	7500	977500	141500	721500			1444
Highest requirement										
	1451	2895								5000

Table 33 : OBDH sizing results per mode

The table clearly shows that the Operational mode is the most demanding in terms of data handling and processing, as all subsystems (excluding the payload) are active during this mode.

A suitable CPU for this task is the TRW RS-3000, which has a total memory of 16 MB (ROM + RAM) and a performance of 10 MIPS (in 32-bit words). The rationale behind the selection of this CPU is driven by its compliance with the memory and performance requirements, as well as its radiation hardness level, which is *Rad Hard* (radiation hardened), the highest achievable level. This is particularly important considering that one of the drivers of the GIOVE-A mission is to characterize the MEO environment, known for its high levels of radioactivity.

The actual on board computer used on GIOVE-A satellite is the *OBC386*^[87] which is a reliable component with a great heritage for LEO missions and has up to 128 MB of total memory. The total required memory found from the sizing (4.3 MB) is much lower than the memory we can find on the actual OBC used. The reason for this discrepancy can be found both in the uncertainties linked to the statistical analysis and, above all, in the assumption that the payload runs on its own different CPU. Clearly it is not the case, and the missing memory from the sizing is probably the one needed to handle the payload data and processing operation

References

- [1] Dominique Detain (ESA). *The First Galileo Satellites: GIOVE*.
- [2] B. kl. Schlaremann, M. Falcone, J. Hahn, and M. Hollreiser (ESA). *The Giove Mission - A Major Step Towards Galileo*.
- [3] J. Benedicto, G. Gatti, John Paffet, Andy Bradford, C. Jackson, and E. Rooney (ESA). *The Triumph of GIOVE-A*. URL: https://www.esa.int/esapub/bulletin/bulletin127/bul127i_benedicto.pdf.
- [4] Giuseppe Mandorlo (ESA). *GIOVE-A Lessons Learned*.
- [5] S. Blair (ESA). *Birth of the European Satellite Navigation Constellation*.
- [6] Michelangelo Ambrosini (EUMETSAT). *Advanced Galileo In-Orbit Validation Constellation Simulations*. URL: https://www.researchgate.net/publication/%5C281096452_Advanced_Galileo_In_Orbit_Validation_Constellation_Simulations.
- [7] eoPortal. *GIOVE-A (Galileo In-Orbit Validation Element-A)*. 2012. URL: <https://www.eoportal.org/satellite-missions/giove-a#spacecraft%205>.
- [8] Andy Brandford, Philip Davies, Doug Liddle, Martin Sweeting, and Wies Tondryk (Surrey Satellite Technologies Ltd). *The GIOVE Small Navigation System*.
- [9] Fabien Droz, Gérald Barmaverain, Qinghua Wang, Pascal Rochat (Temex Neuchâtel Time SA), Francesco Emma, and Pierre Waller (ESA). *Galileo Rubidium Standard. Lifetime data and GIOVE-A related telecommunications*.
- [10] M. Cresci (ESA). *Galileo Workshop - Sensor Station Characterization - Lesson Learned for Risk Mitigation*. Mar. 2007.
- [11] G. Gatti, V. Alpe, M. Malik (ESA), A. Bradford, P. Davies, and E. Rooney (Surrey Satellite Technologies Ltd). *GIOVE-A Satellite e Payload Overview*.
- [12] Andrew Simsky, David Mertens, Jean-Marie Sleewaegen, Belgium) Tom Willems (Septentrio Satellite Navigation, Martin Hollreiser, and Massimo Crisci (ESA). *Multipath and Tracking Performance of Galileo Ranging Signals Transmitted by GIOVE-A*.
- [13] European Space Agency. *Galileo prototype GIOVE-A switched off after 16 years in orbit*. URL: https://www.esa.int/Applications/Navigation/Galileo_prototype_GIOVE-A_switched_off_after_16_years_in_orbit.
- [14] Surrey Satellite Technology. *GIOVE-A, Galileo Pathfinder Satellite, De-commissioned after 16 Years of In-Orbit Service*. URL: <https://www.sstl.co.uk/media-hub/latest-news/2021/giove-a,-galileo-pathfinder-satellite,-de-commissioned-after-16-years-of-in-orbit-service>.
- [15] European Space Agency. *Mission accomplished for Galileo's pathfinder GIOVE-A*. URL: https://www.esa.int/Applications/Navigation/Mission_accomplished_for_Galileo_s_pathfinder_GIOVE-A.
- [16] Philip E. DEVIES (Brunel University). *The GIOVE-A small navigation mission, 'The first satellite in space'*.
- [17] Dave Gibbon, Ian Coxhill, and Mick Drube. *The design, Build Test and In-Orbit Performance of the Giove-A Propulsion System*. 5th International Spacecraft Propulsion Conference, Crete, 2008. 2008.
- [18] Marotta srl. *MV602 SOLENOID VALVE — DATASHEET*. URL: <https://marotta.com/wp-content/uploads/2020/09/MV602.pdf>.
- [19] D. Darfilala and UK) D. Gibbon (Surrey Satellite Technology Ltd. *Ground and flight tests of AlSat-1B butane propulsion system*.
- [20] Federico Romei, Angelo N. Grubisic, Dave Gibbon, Remi A. Herfort, Graham T. Roberts, and UK) Oliver Lane (Surrey Satellite Technology Ltd. *A Thermo-Fluidic Model for a Low Power Xenon Resistojet*.
- [21] *Datasheet S-Band Patch Antennas*. URL: <https://web.archive.org/web/20130202202517/http://www.sstl.co.uk/%20Products/Subsystems/Communication/Antennas/S-Band-Patch-Antenna>.
- [22] *Datasheet S-Band Receiver*. URL: <https://web.archive.org/web/20130119093955/http://www.sstl.co.uk/%20%5C%5CProducts/Subsystems/Communication/Receivers/Transmitter/S-Band-Receiver>.
- [23] *Datasheet S-Band Transmitter*. URL: <https://web.archive.org/web/20130119094716/http://www.sstl.co.uk/%20%5C%5CProducts/Subsystems/Communication/Receivers/Transmitter/S-Band-Transmitter>.
- [24] B. kl. Schlarmann, M. Falcone, J. Hahn, and M. Hollreiser (ESA). *THE GIOVE MISSION – A MAJOR STEP TOWARDS GALILEO*.

- [25] Marco Falcone (ESA). *GIOVE-A : An opportunity for GPS/Galileo Receivers Early Validation.*
- [26] M. Lisi, S. Matussi, R. Lumb, P. Dawkins, and M. Navarroli (ESA). *Galileo Concept of Operations, First IOV LEOP and Initial Operations.*
- [27] URL: [https://documentation.meraki.com/MR/Wi-Fi%5C_Basics%5C_and%5C_Best%5C_Practices/Signal-to-Noise%5C_Ratio%5C_\(SNR\)%5C_and%20%5C_Wireless%5C_Signal%5C_Strength](https://documentation.meraki.com/MR/Wi-Fi%5C_Basics%5C_and%5C_Best%5C_Practices/Signal-to-Noise%5C_Ratio%5C_(SNR)%5C_and%20%5C_Wireless%5C_Signal%5C_Strength).
- [28] Andy Bradford, Philip Davies, Doug Liddle, John Paffett, Prof. Sir Martin Sweeting, Wies Tondryk (Surrey Satellite Technology), Giuliano Gatti, and Antonio Garutti (ESA). *THE GIOVE-A SMALL NAVIGATION MISSION.*
- [29] Leonardo. *Infrared Earth Sensor.* URL: [https://space.leonardo.com/documents/16277711/19573585/IRES_NE_Attitude_Control_Sensors_LQ_mm07787_.pdf?t=1538987566453#:~:text=IRES%20is%20a%20two%20axis,MEO%20\(Medium%20Earth%20orbit\)..](https://space.leonardo.com/documents/16277711/19573585/IRES_NE_Attitude_Control_Sensors_LQ_mm07787_.pdf?t=1538987566453#:~:text=IRES%20is%20a%20two%20axis,MEO%20(Medium%20Earth%20orbit)..)
- [30] SSTL. *2-axis dc/m sun sensor.* URL: <http://www.sstl.co.uk/getattachment/dadecfcb-e1e0-4ddf-91c6-f046a5441be1/Sun-Sensor>.
- [31] EMCORE Corporation. *QRS11 Quartz MEMS Angular Rate Sensor Datasheet.* URL: <http://emcore.com>.
- [32] SSTL. *SSTL Smallsat Wheels.* 2013. URL: <https://web.archive.org/web/20130203211923/http://www.sstl.co.uk/getattachment/8ccf207d-1ada-4bfc-a21b-5c400a1f5d52/SmallWheel>.
- [33] SSTL. *Magnetorquer - MTR-30.* URL: <http://www.sstl.co.uk/getattachment/189dd4b3-214d-4e4b-b52e-d666a7ea1410/MTR-30>.
- [34] SSTL. *Low Power Resistojet.* 2013. URL: <https://web.archive.org/web/20130621211053/http://www.sstl.co.uk/getattachment/9deb85e0-a017-4915-8feb-ce30d4819752/Low-Power-Resistojet>.
- [35] J. D. Liddle, W. Tondryk L. Edge, D. Peilow, and A. Garutti. "GIOVE-A and GMP: SSTL's MEO and GEO Satellite Family – First In-Orbit. Test Results". In: () .
- [36] D.G. Dungate, M.C. Pigg, D. Gittins, S. Hardacre, D. Liddle, and X. Lefort. "GSTB-V2/A NORMAL MODE AOCS DESIGN". In: (17-20 October 2005).
- [37] Prof. Michèle R. Lavagna. *Lecture Notes of Space System Engineering and Operation.* 2023-2024.
- [38] Scott R. Starin, NASA Goddard Space Flight Center John Eterno, and Southwest Research Institute. "Attitude Determination and Control Systems". In: () .
- [39] Dave Gibbon, Ian Coxhill, and Mick Drube. "The design, Build Test and In-Orbit Performance of the Giove-A Propulsion System". In: () .
- [40] International Laser Ranging Service. *Center of Mass Information.* 2015. URL: https://web.archive.org/web/20240420155810/https://ilrs.cddis.eosdis.nasa.gov/missions/satellite_missions/past_missions/gioa_com.html.
- [41] Prof. Franco Bernelli Zazzera. "Lecture Notes of Spacecraft Attitude Dynamics". In: (2023-2024), pp. 62–81.
- [42] SSTL. *Solar Array Drive Mechanism.* URL: <https://web.archive.org/web/20180505212027/http://www.sst-us.com:80/getfile/b6f8a873-e0d5-4aaa-ac08-8e46fb29f897>.
- [43] National Aeronautics and Space Administration. *State-of-the-Art of Small Spacecraft Technology: Thermal Control.* Feb. 2024. URL: <https://www.nasa.gov/smallsat-institute/sst-soa/thermal-control/#7.2.4>.
- [44] NASA. *NASA CERES Project.* URL: <https://ceres.larc.nasa.gov/>.
- [45] URL: <https://www.spaceweatherlive.com/en/auroral-activity/top-50-geomagnetic-storms.html>.
- [46] SSTL. *S-Band Patch Antenna.* URL: <http://www.sstl.co.uk/getattachment/6c88ca87-0802-45e7-bfb6-356336ff710a/S-Band-Patch-Antenna>.
- [47] SSTL. *On-board Data Handling: OBC 386.* URL: https://web.archive.org/web/20041121071407/http://www1.sstl.co.uk:80/datasheets/Subsys_obc386.pdf.
- [48] SSTL. *Butane propulsion system.* URL: <https://web.archive.org/web/20130622031050/http://www.sstl.co.uk/getattachment/aa183d63-ae78-48ff-81f6-cbb16b352249/Butane>.
- [49] SSTL. *Small Satellite Power System.* URL: <http://www.sstl.co.uk/getattachment/fb984708-a8d0-4cc5-9253-49541bf85151/Power-System>.
- [50] SSTL. *Smallsat wheels.* URL: <http://www.sstl.co.uk/getattachment/8ccf207d-1ada-4bfc-a21b-5c400a1f5d52/SmallWheel>.

- [51] SSTL. *Magnetometer*. URL: <https://web.archive.org/web/20130622034304/http://www.sstl.co.uk/getattachment/3b64658e-a81d-46da-97c1-ee43c602b3da/Magnetomer>.
- [52] Keith A. Ryden, Clive S. Dyer, Paul A. Morris, Robert A. Haine, and Susan Jason. "THE MERLIN SPACE WEATHER MONITOR AND ITS PLANNED FLIGHT ON THE GALILEO SYSTEM TESTBED SATELLITE (GSTB-V2/A)". In: *Space Weather* (2005).
- [53] SSTL. *S-Band uplink receiver*. URL: <https://web.archive.org/web/20130119093955/http://www.sstl.co.uk/%20%5C%5CProducts/Subsystems/Communication/Receivers/Transmitter/S-Band-Receiver>.
- [54] SSTL. *S-Band downlink transmitter*. URL: <https://web.archive.org/web/20130119094716/http://www.sstl.co.uk/%20%5C%5CProducts/Subsystems/Communication/Receivers/Transmitter/S-Band-Transmitter>.
- [55] Airbus defence and space. *Rubidium Atomic Frequency Standard*. URL: https://satcatalog.s3.amazonaws.com/components/390/SatCatalog_--.
- [56] Dave Gibbon, Ian Coxhill, and Mick Drube. *The design, Build Test and In-Orbit Performance of the GIOVE-A Propulsion System*. 5th International Spacecraft Propulsion Conference, Crete, 2008. 2008.
- [57] Giuseppe Madorlo. *Giove-A Lessons Learned*. 2007. URL: http://www.giove.esa.int/images/userpage/GIOVE_A_In_Orbit_Lessons_Learned.pdf.
- [58] Andy Bradford, Philip Davies, Giuliano Gatti, Antonio Garutti, Doug Liddle, John Paffett, Prof Sir Martin Sweeting, and Wies Tondryk. *The GIOVE-A small navigation mission*. 20th Annual AIAA/USU Conference on Small Satellites. 20.
- [59] SSTL. *Low Power Resistojet, Datasheet*. URL: <http://www.sstl.co.uk/getattachment/9deb85e0-a017-4915-8feb-ce30d4819752/Low-Power-Resistojet>.
- [60] Javier Benedicto Giuliano Gatti Antonio Garutti John Paffet Andy Bradford C. Jackson E. Rooney. *The Triumph of GIOVE-A*. 2006.
- [61] SQUID3 Space. *SQUID3 OPTICAL SOLAR REFLECTORS*. URL: https://satcatalog.s3.amazonaws.com/components/1449/SatCatalog_-_SQUID3_Space_-_SQ-1_Optical_Solar_Reflector-_Datasheet.pdf?lastmod=20240416124335.
- [62] Mod-Tronic. *Polyimide (Kapton™) Thermofoil Flexible Heaters*. URL: <https://mod-tronic.com/polyimide-thermofoil-heaters.html>.
- [63] TC-TTK-2436. *K type Thermocouple*. URL: <https://customthermoelectric.com/k-type-thermocouple-24-gauge.html>.
- [64] Texas Instruments. *ADS1115*. URL: <https://www.ti.com/product/ADS1115#description>.
- [65] James R. Wertz and Wiley J. Larson. *Space Mission Analysis and Design (Space Technology Library)*. 1999.
- [66] J. D. Liddle, L. Edge, W. Tondryk, D. Peilow, and A. Garutti. *GIOVE-A and GMP: SSTL's MEO and GEO Satellite Family – First In-Orbit Test Results*. 24th AIAA International Communications Satellite Systems Conference - San Diego, California. June 2006.
- [67] S. Craig Clark, H. Alan Weinberg, W. Kevin Hall, and Antonio Garutti. *The Design and Performance of a Power System for the Galileo System Test Bed*. May 2024. URL: <https://ui.adsabs.harvard.edu/abs/2005ESASP.589E...3C/abstract>.
- [68] G. Gatti, A. Garutti, G. Madorlo, J. Paffet, A. Bradford, and E. Rooney Guildford. *The GIOVE-A Satellite: From Design to in-orbit Commissioning*. URL: https://web.archive.org/web/20120304034835/http://www.giove.esa.int/images/userpage/GIOVE_A_Satellite_From_Design_to_in_orbit_Commissioning_ION_GNSS_2006.pdf.
- [69] *Galileo GIOVE-A MEORAD Results and Analysis*. 2008.
- [70] P. Valle, M. Zolesi, A. Netti, A. Rosa, A. Pantano M. Bandinelli, and R. Guidi. *The Design, Modeling and Development of WRAS Antenna for GALILEOSAT*. URL: https://www.researchgate.net/publication/265007342_The_Design_Modeling_and_Development_of_WRAS_Antenna_for_GALILEOSAT.
- [71] SSTL. *Solar Panel solar cell assembly*. URL: https://web.archive.org/web/20120130140518/http://www-personal.umich.edu/~btcesul/SENG_631_files/Subsys_Solar.pdf.
- [72] URL: [https://www.honeycombpanels.eu/en/products/honeycomb/aluminium#:~:text=Honeycomb%20density%20\(from%2020%20to,thickness%20and%20on%20cell%20size](https://www.honeycombpanels.eu/en/products/honeycomb/aluminium#:~:text=Honeycomb%20density%20(from%2020%20to,thickness%20and%20on%20cell%20size).
- [73] URL: <https://physics.nist.gov/cgi-bin/Star/compos.pl?matno=014>.

- [74] Selex EX. *Space photovoltaic sheet.*
- [75] *One Year in Orbit.* 2008.
- [76] Clyde Space Ltd. *SMALLGEO POWER datasheet.* URL: <https://web.archive.org/web/20111122120811/http://www.clyde-space.com:80/documents/33>.
- [77] S. Riva et al. *THE ADM AEOLUS SOLAR ARRAY.* URL: <https://articles.adsabs.harvard.edu/pdf/2008ESASP.661E..20R>.
- [78] DM. Lisi, S. Matussi, R. Lumb, P. Dawkins, and M. Navarroli. *Galileo Concept of Operations, First IOV LEOP and Initial Operations.* SpaceOps 2012 - Stockholm, Sweden. June 2012.
- [79] SSTL. *Solar Array Drive Mechanism.* URL: <https://web.archive.org/web/20180505212027/http://www.sst-us.com:80/getfile/b6f8a873-e0d5%204aaa-ac08-8e46fb29f897>.
- [80] J.C. Chiarini, C. Mathew, H.P. Honold, and D. Smith. *A Satellite for the Galileo Mission.* Conference Paper. 2008.
- [81] Andy Bradford, Philip Davies, Giuliano Gatti, Antonio Garutti, Doug Liddle, John Paffett, Prof Sir Martin Sweeting, and Wies Tondryk. *The GIOVE-A small navigation mission.* 20th Annual AIAA/USU Conference on Small Satellites. 2006.
- [82] iusepppe Mandorlo. *Giove-A Lessons Learned.* 2007. URL: http://www.giove.esa.int/images/userpage/GIOVE_A_In_Orbit_Lessons_Learned.pdf.
- [83] Mahamod Ismail. *TiungSAT-1 OBC386 QNX® SOFTWARE DEVELOPMENT.* URL: <https://web.archive.org/web/20030802135852/http://www.atsb-malaysia.com.my:80/book1/CHAPTER-6.pdf>.
- [84] Chris Plummer Peter Roos Luca Stagnaro. *CAN Bus as a Spacecraft Onboard Bus.* URL: https://www.researchgate.net/publication/234203398_CAN_Bus_as_a_Spacecraft_Onboard_Bus.
- [85] Renesas. *Using CAN Bus Serial Communications in Space Flight Applications.* URL: <https://www.renesas.com/us/en/document/wlp/using-can-bus-serial-communications-space-flight-applications#:~:text=Advantages%20of%20Using%20CAN%20in%20Space%20Applications&text=the%20CAN%20two%2Dwire%20broadcast,by%2010%25%20to%2018%25..>
- [86] G.Gatti A. Garutti G. Mandorlo J. Paffet A. Bradford E.Rooney. *The GIOVE-A Satellite: From Design to in-orbit Commissioning.*
- [87] *On-board Data Handling:OBC 386.* URL: https://web.archive.org/web/20041121071407/http://www1.sstl.co.uk:80/datasheets/Subsys_obc386.pdf.